
A census of Meddies in a long-term high-resolution simulation

Ana Cláudia Barbosa Aguiar^{a,*}, Álvaro Peliz^b, Xavier Carton^c

^a Centro de Oceanografia, Faculdade de Ciências, Universidade de Lisboa, Campo Grande, 1749-016 Lisboa, Portugal

^b Instituto Dom Luiz, Faculdade de Ciências, Universidade de Lisboa, Campo Grande, 1749-016 Lisboa, Portugal

^c Laboratoire de Physique des Océans, UMR6523 CNRS/IFREMER/UBO, UFR Sciences, Brest, France

*: Corresponding author : Ana Cláudia Barbosa Aguiar, email address : aaaguiar@fc.ul.pt

Abstract:

The output from a high-resolution two-decade long Mediterranean Outflow simulation is analysed here to provide a census of Mediterranean Water eddies (aka Meddies), both anticyclones and cyclones. The formation rate of Meddies that survive for at least 90 days is of 12 Meddies yr⁻¹ of which ~12% are cyclones. The rate of formation reaches 40 Meddies yr⁻¹ (30% cyclones) when considering all the Meddies living over 15 days. About 70% of the population is born along the southwestern Iberian slope, but several robust Meddies also originate in points of convergence of the main pathways into the open ocean. The longest-lived Meddies propagate northwestwards, but most of the anticyclones veer southwestwards after a while. As the Meddies drift away from their birthplace, their radius tends to increase gradually from 15 to 30 km. The thickness (depth-difference between isopycnals 27.2 and 27.5) of anticyclones born near Cape St. Vincent contracts by approximately 100 m, after travelling 1000 km from their source; their mean swirl velocities range from about 21 cm s⁻¹ (at z = 1000 m) up to 27 cm s⁻¹ (at z = 600 m). Mean salinity and temperature anomalies are significantly lower for cyclones, which in general are also more slowly rotating, shallower and thinner than anticyclones. Cyclones are more easily tracked at 600 m depth where longer trajectories are recorded. In the vicinity of Portimão Canyon, cyclones outnumber anticyclones while the reverse happens downstream of Cape St. Vincent.

Highlights

► 40 (12) Meddies/yr, 30% (12%) cyclones, living a minimum of 15 (90) days ► 30% of Meddies originate far from the slope in convergence points of main pathways ► Asymmetric distribution of anticyclones/cyclones with respect to Cape St. Vincent ► Long-lived Meddies propagate NW; cyclones more easily tracked at 600 m ► Meddies' radius increases and thickness contracts as they move away from slope

1 **1. Introduction**

2 Through the Strait of Gibraltar, warm and salty waters from the Mediter-
3 ranean Sea spread into the North Atlantic ocean, flowing as a density current
4 at intermediate depths along the southern Iberian slope. The Mediterranean
5 Outflow is partitioned in two main cores: the Upper Core at depths between
6 600 and 1000 m and the Lower Core at depths between 1000 and 1300 m
7 (Ambar et al., 2008, e.g.). Occasionally, it is also possible to discern a Shal-
8 low Core at depths between 400 and 600 m (Ambar, 1983, e.g.) and another
9 denser and deeper branch known as the Deep Core. The latter is confined
10 to a bottom trapped vein (1300–1600 m) found in the vicinity of Portimão
11 Canyon (e.g. Bower et al. (2002); Ambar et al. (2008)).

12 A strong salinity anomaly in the 600–1500 m depth range exists in a more
13 or less triangular region, the Mediterranean salt tongue, based on the western
14 Iberian Peninsula shelf. This feature dominates the thermohaline structure
15 of the Northeastern Atlantic. The shape of this feature coincides roughly
16 with the distribution of sub-surface vortices that carry Mediterranean Water
17 (MW) away into the open ocean. Indeed, the circulation in the Mediter-
18 ranean salt tongue is dominated by advection and diffusion processes.

19 The vast majority of the observed Meddies are anticyclones and usually
20 only anticyclones are referred to as Meddies. However, several observations
21 revealed the existence of cyclonic eddies containing MW and estimated to
22 account for about 30% of the population (Richardson et al., 2000). Hence-
23 forth, both types of eddies will be uniquely referred to as *Meddies*. These
24 are characterised by a central core region with strong temperature and salin-
25 ity anomalies and in approximate solid body rotation. Typical radii range
26 from 10 km (Bower et al., 1997) to 60 km (Richardson and Tychensky, 1998)
27 and the larger ones are usually older too. While anticyclones exhibit a core
28 that can extend from 500 m down to 1500 m, cyclones tend to be shallower
29 vortices with their core centered at about 600 m (Carton et al., 2002). Such
30 aspect ratio gives them a flattened, lens-like three-dimensional shape. For
31 both eddy polarities, records indicate maximum swirl velocities of 30 cm
32 s⁻¹ near the central depth of the core. Nevertheless, the velocity field of
33 these structures usually extends over a large portion of the water column,
34 further than their thermohaline anomalous core. They are sensitive to sharp

35 changes in topography which helps to steer them but may also trigger their
36 disruption.

37 Mediterranean Water lenses are largely formed by instability of the Mediter-
38 ranean Outflow, but they may also originate by interaction of MW filaments
39 with seamounts, currents or surface-intensified eddies. There are several hy-
40 pothesis of generation processes and the details are not totally clear. These
41 include separation of a frictional boundary layer (D’Asaro, 1988; Bower et al.,
42 1997), topographic or coastal effects such as those of capes (Pichevin and Nof,
43 1996; Chérubin et al., 2000; Serra et al., 2002; Serra and Ambar, 2002; Serra
44 et al., 2005) and baroclinic instability of a density current (Chérubin et al.,
45 2007; Duarte et al., 2011). Estimates of the rates of formation near Cape St.
46 Vincent and Estremadura Promontory (see Figure 1) are of 10 and 7 Med-
47 dies per year, respectively (Bower et al., 1997). More recent studies (Carton
48 et al., 2002; Ambar et al., 2008; Carton et al., 2010) have identified Meddies
49 in the Gulf of Cadiz, concluding that Meddies will also frequently detach
50 from the Mediterranean Outflow near the Portimão Canyon. Demidov et al.
51 (2012) suggest a figure of 20–25 lenses per year, for generation over the whole
52 Iberian Coast – the highest guess among the literature.

53 These vortices are believed to play a significant role in sustaining the
54 aforementioned Mediterranean Salt tongue and have been the subject of sev-
55 eral studies (mostly *in situ*) over the last three decades, e.g. Richardson et al.
56 (1989); Bower et al. (1997); Richardson et al. (2000); Ambar et al. (2008);
57 Demidov et al. (2012). However, the available data are rather sparse in space
58 and time, rendering it difficult to weigh in their total contribution towards
59 the salinification of the North Atlantic.

60 Efforts have been made to model the formation of Meddies, using either
61 idealised simulations (Aiki and Yamagata, 2004, e.g.) or more realistic mod-
62 els at regional and global scales (Jungclaus and Mellor, 2000; Serra et al.,
63 2005; Drillet et al., 2005). These studies attained promising results but were
64 hampered by either the reduced size of domain or low resolution, short pe-
65 riod of simulation, and not very accurate boundary conditions at the Strait
66 of Gibraltar. For instance, in Drillet et al. (2005) the Meddies simulated tend
67 to be colder and fresher, and 15% are larger than reported by observations.

68 Here, the Mediterranean Outflow is reproduced numerically in the best
69 possible way given the forceful parametrization of mixing processes at small
70 scales. Atmospheric forcing is included. The highest realism is achieved after
71 using the most suitable boundary conditions at the Strait of Gibraltar. The
72 latter were supplied by another numerical study focused in the exchanges

73 between the Mediterranean Sea and the Atlantic (Peliz et al., 2013). The
74 simulation analysed here has a spatial resolution of about 3 km and covers
75 a period of 20 years, allowing for a thorough study of the population of
76 Meddies.

77 **2. Model Description**

78 *2.1. The Ocean Model, Domain and Configuration*

79 The simulations were performed using the Regional Ocean Modeling Sys-
80 tem (ROMS), which is a community model designed for regional realistic
81 applications (Shchepetkin and McWilliams, 2005). ROMS kernel is a 3D
82 free-surface, sigma-coordinate, split-explicit primitive equation model with
83 Boussinesq and hydrostatic approximations. ROMS has been extensively
84 used in many regional applications including the Gulf of Cadiz (Peliz et al.,
85 2007, 2009, 2013).

86 The model’s grid (Figure 1) has a ~ 3 km horizontal spacing that is $\sim 1/3$
87 of the radius of the smallest Meddies which are thus properly resolved. To
88 ensure a reasonable resolution near the bottom, which is important for an
89 adequate simulation of the outflow on the Gulf of Cadiz slope, the grid has
90 32 sigma vertical levels with a moderate surface stretching of $\theta_s = 4$ ($\theta_b = 0$);
91 see Shchepetkin and McWilliams (2005) and Hedström (2009) appendix B
92 for a detailed description of ROMS vertical coordinates. An alternative way
93 of increasing the near-bottom resolution is to use $\theta_b \neq 0$. However, the
94 latter would increase the steepness of the sigma layers and, consequently,
95 increase the pressure gradient errors (Shchepetkin and McWilliams, 2003).
96 The baroclinic time-step δt is 300 s, and the fast barotropic mode is $\delta t/40$ s.

97 *2.2. Boundary Conditions*

98 The open boundary conditions consist of a combination of radiation and
99 flow-adaptive nudging toward prescribed values from climatology as described
100 in Marchesiello et al. (2001). Monthly climatologies of temperature and salin-
101 ity, together with geostrophic and Ekman velocities (calculated from monthly
102 averaged stratification and surface winds) are used on the boundary as pas-
103 sive/active conditions (Marchesiello et al., 2001). Nudging to climatological
104 values is made with different coefficients for inward (1 day for momentum
105 and 10 days for tracers)/outward flow (360 days for tracers and momentum).
106 Across the nudging/sponge band, the nudging progressively decays to zero
107 in the interior within a band of 50 km also used for the sponge (see below

108 Section 2.3). The initial and open boundary temperature and salinity fields
109 were taken from the WOA 2005 (Locarnini et al., 2006; Antonov et al., 2006)
110 for the southern, western and northern open boundaries. The eastern open
111 boundary was subjected to a different treatment. In order to force an outflow
112 that is as realistic as possible, the climatology was produced with the output
113 from Peliz et al. (2013).

114 For the barotropic mode we use Orlansky-type radiative conditions to-
115 gether with volume conservation. ROMS volume conservation condition con-
116 sists of diagnosing the mass imbalance at each time step (by integrating all
117 the barotropic transport along the domain perimeter). In case of loss of vol-
118 ume, a correction is applied, dividing the excess/deficit by all cells along the
119 open boundaries and forcing this mass out/in as a volume compensation. A
120 correct implementation of this conservation condition, in a domain covering
121 the Atlantic and Mediterranean, requires that this condition is applied to
122 each basin separately. Otherwise, the mass compensation induces unwanted
123 and spurious barotropic fluctuations at the strait that sometimes are well
124 above the observed values. In this configuration, we proceed with the sep-
125 aration of the volume condition as described in Peliz et al. (2013). At each
126 time step the barotropic transport was calculated for the Atlantic side (Q_{Atl})
127 and for the Mediterranean (Q_{Med}), independently. Next, assuming volume
128 conservation, we force the transport entering/leaving on the Atlantic bound-
129 ary to be equal to the transport leaving/entering on the open boundary in
130 the Mediterranean side and this transport should equal Q^t , the net (physi-
131 cal) mass transport through the strait (~ 0.05 Sv). This approach ensures
132 volume conservation and the needed sub-inertial barotropic transport across
133 the strait. Internally, the model is free to produce the required baroclinic
134 adjustment (the inflow/outflow) to this external barotropic forcing.

135 *2.3. Numerical Options and Parametrization of the Strait Processes*

136 A third-order upstream-biased accurate predictor-corrector - leapfrog/Adams-
137 Moulton - time step algorithm (Shchepetkin and McWilliams, 2005) is used
138 for momentum and tracers. In some circumstances, this tracer advection
139 scheme produces spurious diapycnal mixing (Marchesiello et al., 2009), that
140 may lead to substantial erosion of internal structure in low resolution ex-
141 periments. In finer resolution simulations, this spurious mixing, although
142 inescapable, is not expected to significantly degrade the thermohaline char-
143 acteristics despite contributing for smoother thermohaline structures.

144 Due to the dispersive properties of the advection equation, the simulations
145 can be conducted with reduced or null explicit mixing. Null mixing is applied
146 everywhere except in the sponge layer, where Laplacian viscosity is used and
147 the coefficient is set to ramp up from zero in the innermost cell to 200 m^2
148 s^{-2} on the outermost cell. The sponge is as wide as the nudging band.

149 Vertical mixing processes are parametrised with the non-local K-profile
150 (KPP) boundary layer scheme (Large et al., 1994) implemented for both
151 surface and bottom boundary layers. The vertical diffusion terms are treated
152 with a semi-implicit Crank-Nicholson scheme to avoid time step restrictions,
153 due to large vertical mixing rates in the boundary layers and also in the
154 interior when static stability needs to be restored. A uniform and constant
155 quadratic bottom drag coefficient of 3.5×10^{-3} is used.

156 Since the details of the mixing processes and entrainment of the outflow
157 are not explicitly resolved at these resolutions, a localised spot of increased
158 mixing and diffusion was created out of the Strait. A Smagorinsky mixing
159 coefficient is calculated and it is multiplied by a space sine function which
160 decays radially within a 30 km zone centered at (35.9°N ; 6.15°W), and in
161 depth using a function based on a hyperbolic tangent that goes to zero for
162 depths above 200 m. This ensures that the mixing spot is very localised
163 laterally and in depth, and is restricted to the lower western part of the
164 channel (35.9°N ; 6.15°W).

165 The flow at the source (Strait) is comparable with observed values (trans-
166 port, and TS characteristics), hence the realism of the mixing processes can
167 be assessed by comparing the simulated water vein with observations at dif-
168 ferent distances from the Strait. This comparison is not illustrated here but
169 it has been done in previous studies, see e.g. Peliz et al. (2013) (Figure 8).

170 *2.4. External Forcing and Topography*

171 Atmospheric forcing is based on momentum and air-sea fluxes monthly
172 climatologies from COADS (da Silva et al., 1994). No tidal forcing was ap-
173 plied. To build the model topography we used two data bases: the global
174 Smith and Sandwell (1997) topography and a local high resolution map de-
175 scribed in Sanz et al. (1991) that covers in detail the Strait of Gibraltar.
176 ROMS requires a significant degree of topography smoothing to avoid steep
177 slopes that induce pressure gradient errors (Shchepetkin and McWilliams,
178 2003, e.g.). This smoothing is usually performed by filtering the initial to-
179 pography (h) with a $\log(h)$ based filter (Penven et al., 2008, e.g.), and in very
180 steep regions (as in the Strait) it may substantially degrade the topography.

181 An iterative procedure to tackle this problem was developed in Peliz et al.
182 (2013) and is applied to the present configuration as well.

183 For a significant part of the work, the preparation of the model’s initial
184 conditions and fields was conducted using the ROMS tools package (Penven
185 et al., 2008).

186 Note that this experiment will not have interannual variability and it is
187 done so in order to ensure that its outcome reflects the intrinsic variability
188 of the system alone.

189 *2.5. Mean Circulation and EKE*

190 Although the study of the mean circulation is out of the scope of this
191 paper, it is instructive to compare the regional circulation features and
192 the mean Eddy Kinetic Energy with those in previous papers. Figure 2
193 shows the time-mean velocity field (u, v) and the eddy kinetic energy $EKE =$
194 $0.5 (\langle (u - \langle u \rangle)^2 \rangle + \langle (v - \langle v \rangle)^2 \rangle)$ at 1000 m depth.

195 In the velocity field, it is possible to recognise the Mediterranean Un-
196 dercurrent (with velocities above 10 cm s^{-1} off Cape St. Vincent), a well
197 pronounced southward flow just west of Gorringer bank ($\sim 12.5^\circ\text{W}$) and a
198 westward zonal flow at $\sim 37.5^\circ\text{N}$, which can also be seen in Bower et al.
199 (2002) (Figure 14c). Features such as the eastern branch of the Azores Cur-
200 rent ($\sim 34^\circ\text{N}$) and the southward recirculation at about 16.5°W , $37 - 39^\circ\text{N}$
201 resemble those observed in Barbosa Aguiar et al. (2011) (Figure 2). Further-
202 more, the cyclonic recirculation pattern seen in the Gulf of Cadiz coincides
203 with that already documented in several studies (Peliz et al., 2007; Kida
204 et al., 2008; Lamas et al., 2010).

205 The larger values of EKE ($> 50 \text{ cm}^2 \text{ s}^{-2}$) are spread out along well known
206 corridors for Meddies: a tongue that veers from Cape St. Vincent into the
207 basin among the Horseshoe seamounts and a zonal band at $\sim 38^\circ\text{N}$. There
208 are also less familiar features: a small branch of moderate $EKE \sim 35 \text{ cm}^2$
209 s^{-2} in the Gulf of Cadiz and a striking “shadow region” at about 37°N ,
210 $15 - 18^\circ\text{W}$. The range of values of EKE is in very good agreement with the
211 observational results shown in Bower et al. (2002) (Figure 14d), while the
212 shape and location of the most energetic region are close but not exactly the
213 same.

214 At 600 m depth (not shown), the same features prevail in both products,
215 albeit with greater intensity.

216 Despite the intended transparency of the open boundaries to the propa-
217 gation of eddies there are still obvious signs of recirculations and rim currents

218 within the sponge band, on the western boundary and southwest corner of the
219 domain. Those, however, do not seem to disturb the interior of the domain
220 and thus should not affect the propagation of eddies therein.

221 The experiment was run for 25 years but only the last 20 years were
222 studied so that the eddy fields analysed correspond to a state of full equilib-
223 rium, after transient processes of adjustment. A more or less regular chain of
224 vortices could be observed, travelling from the slope to the western bound-
225 ary, after the first 5 years of simulation. Time-averaged output fields (sur-
226 face height, velocity, temperature and salinity) were recorded every 3 days
227 ($\delta t_{out} = 3$).

228 3. Identification and Selection of Meddies

229 The task of analysing eddies in such a large dataset demanded the use of
230 an automatic procedure. To identify and track all the eddies that contained
231 MW (Meddies), we decided to run an existing eddy tracking algorithm fol-
232 lowed by a “Meddy verification criteria”.

233 The eddy detection algorithm and its source code were developed by
234 Nencioli et al. (2010). This algorithm has been successfully applied to high-
235 resolution numerical products, e.g. Dong et al. (2012). In Appendix A, there
236 is a description of the procedure of eddy identification and tracking.

237 The algorithm was run separately at $z = 600$ m and $z = 1000$ m lev-
238 els because the dynamical signature of cyclones (C) and anticyclones (AC)
239 should be more intense at each of these depths, as described above in Section
240 1. Therefore, this choice is expected to optimise the detection and tracking
241 of C at $z = 600$ m and AC at $z = 1000$ m, and this was confirmed by our
242 results (Section 4.1.2).

243 After running the eddy tracking algorithm we had to determine which
244 of the detected eddies were Meddies. To do so, we devised a rather simple
245 and flexible criteria based on the depth-averaged salinity anomaly of the
246 eddy’s centre as explained in Appendix B. What distinguishes Meddies
247 from other eddies is not only the higher values of salinity but also the higher
248 temperatures in their cores. However, the salinity anomaly is clearer and for
249 the sake of simplicity, the criterion devised here relies solely on the depth-
250 averaged salinity anomaly of the eddies.

251 Any eddy that retained $\Delta S \geq 0.12$ psu, over more than half of its life-
252 time ($\gamma \geq 0.5$) is considered to be a Meddy. This enabled the detection of

253 robust Meddies even if they exhibited fairly weak salinity anomalies for some
254 time (see e.g. AC in Figure B.11).

255 This apparently low threshold of ΔS is not comparable with those used
256 for the selection of Meddies in observations because it is not computed in
257 the same way. The characteristic salinity anomaly here is a *depth-averaged*
258 *anomaly* of a structure known *a priori* to be an eddy. Historical datasets of
259 observations (Richardson et al., 1991, e.g.) were produced from collections of
260 hydrographic sections not guaranteed to correspond to eddies, hence the need
261 for rather high thresholds referring to the maximum salinity in the section.
262 Many other observational records were gathered by floats seeded directly into
263 the thermohaline core of Meddies, where the anomaly is bound to be very
264 high. Also, the age and life-time of the Meddies surveyed *in situ* are usually
265 unknown, but most of these are likely to be rather young Meddies (high
266 salinity anomaly) which have trapped drifters seeded into the Mediterranean
267 Undercurrent.

268 Our choice of threshold parameters ΔS and Δt is down to a compromise:
269 to avoid the detection of too many spurious eddies (non Meddies), while still
270 able to capture a wide range of Meddies, both weak and strong ΔS and
271 intensified at different depth levels.

272 Note that inhere we are considering all the eddies with a MW core and
273 not only the ones originating directly from Mediterranean Outflow instability.
274 Furthermore, this study only concerns the southwestern part of the Iberian
275 Peninsula and therefore all Meddy generation sites outside this region are
276 excluded. Other possible sites of generation are Cape Ortegal and Cape
277 Finisterre or Galicia Bank (Richardson et al., 1991; Paillet et al., 1999), as
278 well as other locations along the western coast of Iberia north of 41°N.

279 4. Results

280 For an overview of the data, the Meddies are split into different cate-
281 gories according to their life-time (Δt) and degree of salinity anomaly (ΔS),
282 while ensuring $\gamma \geq 0.5$ for all Meddies. The distinction between datasets
283 of Meddies will be made by referring to the values ΔS and Δt (as well as
284 r -parameter and z -level) used in the Meddies selection described in Ap-
285 pendix A and Appendix B.

286 To produce a quantitative analysis, we choose to use the dataset of Med-
287 dies with $\Delta t \geq 90$ days and $\Delta S \geq 0.12$ psu (Figure 3 top) because: i)
288 shorter-lived Meddies will not have enough time to mature and are unlikely

289 to have a significant impact beyond the vicinity of the Iberian slope, and ii)
290 the percentage of cyclones still amounts to nearly 14% allowing for a reason-
291 ably sized sample of cyclones, unlike what happens for higher thresholds of
292 ΔS and Δt .

293 A whole section is dedicated to Meddies born along the Southwestern
294 Iberian slope because these are more likely to form directly from the Mediter-
295 ranean Undercurrent.

296 *4.1. Meddies in the Whole Domain of Study*

297 *4.1.1. Life-times*

298 In Figure 3 (top and centre) are shown all the Meddies born within the
299 whole region of study and surviving for at least 90 or 150 days with $\Delta S \geq 0.12$
300 psu. The overall rate of formation varies between 8 units yr^{-1} for $\Delta t \geq 150$
301 days and 12 units yr^{-1} for $\Delta t \geq 90$ days.

302 Long lived structures are largely anticyclonic. The percentage of cyclonic
303 Meddies reaches 14% among Meddies that survive at least three months, but
304 it decreases to 10% when selecting only Meddies that survive for a minimum
305 of five months. In the whole 20 years of simulation, a maximum of 17 cyclones
306 (detected at $z = 600$ m) survived for at least 150 days with $\Delta S \geq 0.12$ psu.
307 This suggests that nearly one very long-lived cyclone is born every year, while
308 most of the cyclones formed tend to quickly disappear offshore.

309 While long-lived anticyclones form in the western slope, long-lived cy-
310 clones form in the southern slope.

311 Several Meddies originate far from the slope, namely in the lee side of the
312 seamounts Josephine and Ampère but also in the Gulf of Cadiz and Tagus
313 Abyssal Plain (Figure 3 top). It should be noted that these structures are
314 very resilient Meddies that can survive for rather long periods of time.

315 For Meddies with life-times as short as 15 (see Table 4) or 30 days (not
316 shown), the overall rate of formation varies between 40 and 24 units yr^{-1} , of
317 which 30% and 24% are cyclones, respectively.

318 *4.1.2. Sensitivity to Depth Level*

319 Figure 3 confirms that the success of identification of either type of Med-
320 dies is sensitive to the depth levels surveyed. Blue lines (trajectories of C) are
321 more numerous at $z = 600$ m than at $z = 1000$ m (except for $\Delta S \geq 0.3$ psu),
322 and several trajectories are similar in both levels (hence, assumed to corre-
323 spond to the same eddy) but are significantly longer in the first case. The
324 detection of cyclones is generally more successful at $z = 600$ m as expected.

325 This confirms the shallower intensification (maximum horizontal velocity) of
326 cyclones versus anticyclones mentioned in Section 1.

327 On the other hand, for $z = 1000$ m and $\Delta S \geq 0.12$ psu, there are two
328 C-trajectories (finishing in the western border at 36.5°N) which do not match
329 any of the trajectories traced at $z = 600$ m. The same happens for cyclones
330 with $\Delta S \geq 0.3$ psu. This is evidence that cyclonic structures can occasionally
331 be intensified at deeper levels too.

332 *4.1.3. Salinity Anomaly*

333 The trajectories of Meddies with $\Delta t \geq 90$ days and $\Delta S \geq 0.3$ psu are
334 presented in Figure 3 (bottom) and the corresponding rates of formation
335 and percentage of cyclones are in Table 1, along with rates for $\Delta S \geq 0.12$
336 and 0.2 psu. These threshold values were chosen in order to identify long-
337 lived Meddies with strong salinity anomalies, which are likely to be the main
338 carriers of MW to far-off distances.

339 Only about half of the Meddies that mature to three months or beyond
340 have $\Delta S \geq 0.3$ psu. A total of 6 units yr^{-1} were detected at $z = 1000$ m,
341 of which 3.4 units yr^{-1} occur in box II, 0.4 unit yr^{-1} in box I and 0.5 unit
342 yr^{-1} originate near the Josephine seamount (see limits of boxes in Figure 4).
343 Cyclones seldom verify $\Delta S \geq 0.3$ psu and $\Delta t \geq 90$, with only three examples
344 detected at $z = 1000$ m and none recorded at $z = 600$ m (see Figure 3
345 bottom).

346 *4.1.4. Rates of Exit of Meddies into the North Atlantic*

347 In Table 2 are listed the rates of survival into the North Atlantic (exit of
348 the domain) recorded for different sets of Meddies tracked with $r = 18$ km.
349 These correspond to all Meddies whose last record lies within 0.2° of the
350 southernmost, westernmost and northernmost limits considered here. For
351 the Meddies with $\Delta t \geq 90$ days, the rates of survival into open ocean vary
352 between 2.8 and 4.5 units yr^{-1} . The largest percentage of the total eddy
353 population that manages to reach the North Atlantic is about 50%, attained
354 when $\Delta t \geq 90$ days and $\Delta S \geq 0.3$ psu. The latter indicates that the Meddies
355 which are more likely to reach open ocean are those with the largest salinity
356 anomalies.

357 *4.1.5. Properties of Meddies in the Whole Domain*

358 In Table 3 are given the physical characteristics of the Meddies with
359 $\Delta t \geq 90$ days and $\Delta S \geq 0.12$ psu. Results are presented for each type of

360 eddy and level of detection, taking into account the time-mean parameters
361 along each trajectory recorded: 190 AC and 31 C at $z = 600$ m, and 216 AC
362 and 28 C at $z = 1000$ m.

363 From the results in Table 3 it is clear that cyclones are short-lived struc-
364 tures: the results indicate average survival times of only 57 – 64% of the
365 average life-time of anticyclones. Similar results are obtained for the respec-
366 tive total distances travelled. Also, at the level $z = 600$ m, the cyclones can
367 be tracked for longer periods and distances than at $z = 1000$ m.

368 The radii of both AC and C are comparable: the mean radius of AC and
369 C varies between 23 and 27 km, but the largest anticyclone had a radius of
370 64 km whereas the largest cyclone had a smaller radius of 50 km.

371 At both depth-levels analysed, the mean swirl velocities of C are only
372 about 60% of those of AC.

373 For both types of Meddies, the translation velocities are similar and typi-
374 cally about 3 cm s^{-1} , with peak values of $5.2 - 6.2 \text{ cm s}^{-1}$ and minima
375 of $1.1 - 1.7 \text{ cm s}^{-1}$. It should be noted that the eddy detection parameter
376 $r = 18$ km used here imposes a maximum of $V_t \sim 7 \text{ cm s}^{-1}$. The analysis of
377 a dataset of Meddies obtained after running the detection with $r = 36$ km
378 (maximum $V_t \sim 14 \text{ cm s}^{-1}$) revealed that at most 11% of the Meddies would
379 exhibit $V_t \geq 6.5 \text{ cm s}^{-1}$ (not shown).

380 The salinity and temperature values, as well as the respective anomalies,
381 presented in Table 3 are the vertical average over depths between 600 m and
382 1300 m, along the profile of the dynamical eddy’s centre detected at either
383 $z = 600$ m or $z = 1000$ m. While the mean salinity values are very close for
384 each type of eddy, the mean salinity anomalies recorded for C are only about
385 55% of those for AC. The mean and maximum values of temperatures in AC
386 are always about 1°C degree higher than for C, and the mean temperature
387 anomalies of AC ($\sim 1.3^\circ\text{C}$) are also much higher than those of C ($\sim 0.4^\circ\text{C}$). In
388 the dataset presented here, the largest depth-averaged time-mean salinity and
389 temperature anomalies of a Meddy were of 0.57 psu and 2.44°C , respectively,
390 both recorded in Meddies detected at $z = 1000$ m.

391 *4.2. Meddies of the Iberian Slope*

392 *4.2.1. Population, Sites and Rates of Formation*

393 The trajectories of Meddies born along the southwestern Iberian slope
394 during the 20 years of simulation, and surviving for at least 90 days, are plot-
395 ted in Figure 4 (top). The hotspots of coastal formation are found upstream
396 and downstream of Cape St. Vincent within boxes I and II, respectively, but

397 there is also some formation occurring at Setubal Canyon and Estremadura
398 Promontory in box III. The Meddies formation rate for the three boxes al-
399 together is roughly of 8 units yr^{-1} for both depth levels analysed. Box II
400 records the highest formation rate with about 6 units yr^{-1} while in box I
401 this rate is approximately of 1 unit yr^{-1} . When running the eddy detection
402 for $r = 36$ km the rates of generation are slightly lower – the results are
403 summarised in Table 4.

404 The rates of formation are much higher when analysing the Meddies
405 dataset with $\Delta S \geq 0.12$ psu and a life-time threshold of only 15 days (see
406 Table 4). Combining the three boxes, the formation rate reaches 18 units
407 yr^{-1} , with about 9 units yr^{-1} in box II and 5.5 (7.2) units yr^{-1} in box I, for
408 an eddy detection at $z = 600$ m ($z = 1000$ m).

409 By comparing the rates of formation for different regions, it becomes
410 clear that a significant amount of Meddies (nearly half, if $\Delta S \geq 0.12$ psu and
411 $\Delta t \geq 15$ days) are born far from the Iberian slope as observed in Section 4.1.1.

412 The percentage of the population of Meddies with cyclonic rotation varies
413 considerably depending on the formation site considered, as shown by the
414 rather asymmetric distribution of blue lines in Figure 4. While all Meddies
415 (except one at $z = 600$ m) in box II have anticyclonic rotation, the reverse
416 happens in box I where cyclonic Meddies account for 57-91% of the popula-
417 tion (see Table 4). When considering all the Meddies born in boxes I, II and
418 III, the percentage of cyclonic vortices is only about 8-14% if $\Delta t \geq 90$ days,
419 but increases to 27-32% if $\Delta t \geq 15$ days.

420 4.2.2. *Main Paths*

421 The vast majority of slope’s Meddies will initially move northwestwards
422 to the Tagus Abyssal Plain from where they can follow two distinct paths: a
423 “highway” between the Horseshoe seamounts and the Estremadura Promon-
424 tory (at about 38°N) that leads them straight to west, or a “winding path”
425 that leads them southwestward through the Horseshoe seamounts; for topo-
426 graphic references see Figure 1. In the latter case, while some of the Meddies
427 take an exit to west, several others exit to south (where the gaps between the
428 seamounts are wider) and can either turn southwestwards to Madeira Island
429 or continue further south to the Canary Basin with some detours. Right
430 after formation, a minority of Meddies will travel straight to south and may
431 veer eastwards to the Gulf of Cadiz (Figure 4).

432 Meddies born in box I (mostly C) tend to remain in the Gulf of Cadiz
433 throughout their life-time (Figure 4 bottom), but some will also take a

434 southward, northwestward, or even a westward (straight into the Horseshoe
435 seamounts) path.

436 West of $\sim 16^\circ\text{W}$, most of the Meddies travelling westward will eventually
437 turn southwestward following a path more or less along the western border
438 of the Horseshoe seamounts to west of Madeira Island. In a few cases, the
439 trajectories just happen to suddenly veer to the south, e.g. partly meridional
440 trajectories of C and AC at $\sim 16.5^\circ\text{W}$ in Figure 4 ($z = 600$ m), probably
441 under the influence of a southward regional current that can be seen in Fig-
442 ure 2 (top). Furthermore, some cyclones continue to travel westwards or
443 northwestwards through the western border of the domain.

444 By comparing the results for both depth levels surveyed, it is again no-
445 ticeable (see Section 4.1.2) that cyclones can be followed for a longer time
446 (and distance) when tracked at $z = 600$ m – see Figure 4 (top). Also, the
447 percentage of C detected in box I increases by roughly 20% when the eddy
448 detection was ran at $z = 600$ m instead of $z = 1000$ m (see Table 4).

449 *4.2.3. Evolution of Meddies*

450 In Figure 5 is presented a comparison between Meddies born in each
451 box of the Iberian Slope and the evolution of their characteristics as they
452 age and move away from their origin. AC and C were treated separately
453 and the data were not plotted for samples with less than 10 Meddies. At
454 every point of a trajectory, the curvilinear distance to origin was computed
455 as the sum of the distance between each two previous points. The records of
456 all the Meddies were then binned into segments of 40 km, according to the
457 respective distances to origin, and the mean and standard deviation values
458 were computed for each bin. This analysis was done for both levels of tracking
459 but given the similarities, at the exception of swirl velocity, only the results
460 of tracking at $z = 600$ m are shown in Figure 5. The Meddies analysed here
461 correspond to a subset (eddies born in the Iberian Slope) of the Meddies
462 population with $\Delta S \geq 0.12$ psu and $\Delta t \geq 90$ analysed in Table 3.

463 The first chart provides information on the number of records used, il-
464 lustrating that the statistical significance of the data is very heterogeneous
465 given the large differences in the number of Meddies of each type per box.
466 Moreover, the number of records tends to decrease as the distance to origin
467 increases. The values provided for AC from box II are the most statistically
468 significant. Halfway to the origin, the number of records is more or less con-
469 stant at about 500 counts. It peaks at 500 km and then drops to about 300
470 counts at 1000 km. In boxes I and III the number of records reaches about

471 100 counts.

472 The radius of the Meddies tends to gradually increase from about 15 km
473 at birth to values above 25 km (box II) or 30 km (box I) by the end of
474 tracking, about 1000 km away from the source. At $z = 600$ m, C from box I
475 exhibit somewhat larger radii (and standard deviations) than AC from box
476 II, while the reverse happens at $z = 1000$ m (not shown).

477 The thickness (h) of the Meddies was estimated as the difference between
478 the depths of isopycnals 27.2 and 27.5 (with reference to the surface level)
479 along the profile of the eddy's centre. The depth of the maximum of salinity
480 between the same isopycnals (zS_{max}), as well as the depth-averaged salin-
481 ity and temperature anomalies in that depth range ($\langle\delta S\rangle$, $\langle\delta T\rangle$) are also
482 represented in Figure 5.

483 The graphs show that the thickness of cyclones is only about 250-300 m
484 and more or less constant with distance, whereas the thickness of anticyclones
485 varies from $\sim 450 - 500$ m at the origin to $\sim 400 - 430$ m after 1000 km. The
486 depth of the maximum of salinity is always shallower in cyclones ($\sim 600 - 700$
487 m) than in anticyclones ($\sim 800 - 850$ m) where this maximum deepens slightly
488 with distance to origin.

489 Both salinity and temperature anomalies are significantly lower for cy-
490 clones than for anticyclones, and the anomalies from Meddies with origin in
491 box II are typically larger than those in box III. As expected, the salinity and
492 temperature anomalies estimated here (see Appendix B) increase steadily as
493 the Meddies progress into the eastern North Atlantic, translating into fresher
494 and colder background waters.

495 For Meddies of box II the translation velocity (V_t) appears to decrease
496 from 4 to 3 cm s⁻¹ at 500 km away from the origin (perhaps due to topo-
497 graphic obstacles), increasing slightly after that only to drop again to 3 cm
498 s⁻¹ or below at about 850 km.

499 At $z = 600$ m, the swirl velocities (V_s) of AC from box II quickly in-
500 crease from ~ 21 cm s⁻¹ to ~ 27 cm s⁻¹ within the first 100 km, decreasing
501 monotonously to ~ 22 cm s⁻¹ after that. At $z = 1000$ m, the swirl velocity
502 increases initially from ~ 15 cm s⁻¹ to ~ 21 cm s⁻¹, staying roughly constant
503 afterward. These speeds are significantly higher than records concerning the
504 other boxes: $\sim 10 - 20$ cm s⁻¹ at $z = 600$ m and $\sim 6 - 15$ cm s⁻¹ at $z = 1000$
505 m.

506 For illustration purposes only, the mean trajectories (and standard devi-
507 ation of the coordinates) of the Meddies born along the Iberian slope and
508 tracked at $z = 600$ m are plotted in Figure 6. Such schematic highlights

509 the main points of origin and directions followed by the slope Meddies, but
510 it lacks the variety of noticeable bends and routes visible in the spaghetti
511 diagrams of Figure 4.

512 **5. Summary of Simulated Meddies**

- 513 1. Initially, most of the Meddies move northwestwards but then either
514 propagate straight to west or veer southwestward facing a winding path
515 across the Horseshoe seamounts. West of 16°W most of the Meddies
516 turn southwestwards, probably due to the regional currents and the
517 effect of local topography. A few Meddies recirculate in the Gulf of
518 Cadiz.
- 519 2. The longest-lived cyclones propagate northwestwards passing between
520 Josephine and Tore seamounts, never veering southwards. Shorter-lived
521 cyclones either recirculate in the Gulf of Cadiz or travel northwestwards
522 into the Tagus Abyssal Plain. Few cyclones move southwestwards to
523 the Horseshoe seamounts.
- 524 3. In the whole domain of study, the rate of formation reaches 40 Meddies
525 yr^{-1} considering all the Meddies that survived for at least 15 days
526 and whose salinity anomaly value was above 0.12 psu, the lowest value
527 that still classifies the simulated eddies as Meddies. About 30% of the
528 population of Meddies are cyclones. When restricting the analysis to
529 the southwestern Iberian slope, the formation rate is almost halved
530 to 18 Meddies yr^{-1} . The rate of generation around Portimão Canyon
531 varies between 5.5 Meddies yr^{-1} ($z = 600$ m) and 7.2 Meddies yr^{-1}
532 ($z = 1000$ m), being dominated by cyclonic Meddies (84% and 61% in
533 each case). The upper rates near Cape St. Vincent and Estremadura
534 Promontory are respectively of 9.3 Meddies yr^{-1} and 1.4 Meddies yr^{-1}
535 (see Table 4). Note that such a low threshold on the life-time increases
536 the likelihood of counting the same event more than once. Every time
537 the Meddy fails to fulfil the detection criteria only to fulfil it again
538 afterward (more than 6 days later) it will be considered a new event.
- 539 4. When considering only Meddies that survived for at least 90 days, with
540 minimum salinity anomalies of 0.12 or 0.3 psu, the rates of formation
541 drop to about 12 or 6 Meddies yr^{-1} respectively, while the percentage
542 of cyclonic Meddies decreases to 12% or 3%, in the whole domain of
543 study. Several robust Meddies originate on the lee side of Josephine
544 seamount and fewer on Gorringe, Ampère and Lion seamounts.

- 545 5. As the Meddies drift away from their birthplace, their radius tends to
546 increase gradually from 15 to 30 km. After travelling about 1000 km
547 away from its origin, a Meddy's thickness contracts by approximately
548 100 m. The Meddies that form near Cape St. Vincent have mean swirl
549 velocities that range from about 21 cm s^{-1} (at $z = 1000 \text{ m}$) up to ~ 27
550 cm s^{-1} (at $z = 600 \text{ m}$). These velocities are larger than those of Meddies
551 forming around Estremadura Promontory or Portimão Canyon, and the
552 same happens for salinity and temperature anomalies.
- 553 6. Cyclones are more easily tracked at 600 m, where longer trajectories are
554 recorded. Mean salinity and temperature anomalies are significantly
555 lower for cyclones, which in general are also more slowly rotating, shall-
556 lower and thinner than anticyclones. The thickness of cyclones (~ 250
557 m) remains more or less constant throughout their trajectories, unlike
558 the radius that tends to increase slightly.
- 559 7. In general, the population of Meddies born in the vicinity of Portimão
560 Canyon is distinct: cyclonic Meddies outnumber anticyclones (mini-
561 mum salinity anomalies of 0.12 psu) and the few cyclones exhibiting
562 the salinity anomalies above 0.3 psu can only be tracked at depth (1000
563 m). However, a comparison of physical properties of Meddies formed
564 upstream and downstream of Cape St. Vincent provided ambiguous
565 results.

566 6. Discussion

567 6.1. Formation and Main Paths of Meddies

568 Several sites of formation of Meddies have been identified here: Portimão
569 Canyon, Cape St. Vincent, Estremadura Promontory and the lee-side of sev-
570 eral Horseshoe seamounts. Two different snapshots of vorticity and salinity
571 fields at $z = 1000 \text{ m}$ are shown in Figures 7 and 9 to illustrate an instant of
572 the spatial distribution of MW lenses. Note the prominent string of vortices
573 off Cape St. Vincent in Figure 7. The main paths chosen by Meddies co-
574 incide with regions of enhanced EKE (Figure 2 bottom) due to the stirring
575 effects of Meddies (Bower et al., 2002).

576 Although Portimão Canyon has only been confirmed as a source of Med-
577 dies in the last 10 years (Serra and Ambar, 2002; Carton et al., 2002; Serra
578 et al., 2005), Cape St. Vincent and Estremadura Promontory have been rec-
579 ognized as such since Zenk et al. (1992) and Bower et al. (1997). There is
580 prevalence of similarly shaped trajectories of both anticyclones and cyclones

581 in the Gulf of Cadiz and the formation of a dipole is evident in Figure 8. In
582 that figure, two poles of positive and negative vorticity correspond to two re-
583 lative maxima of salinity. This confirms the hypothesis of dipole-generation
584 off the Portimão Canyon already discussed by several authors (Serra and
585 Ambar, 2002; Ambar et al., 2008; Carton et al., 2010). However, dipole
586 structures are not exclusive to the southern Iberian slope and can be seen
587 elsewhere, e.g. in Figure 9 there is another dipole forming off Estremadura
588 Promontory.

589 Beforehand, the only seamount reported to be another birth place of Med-
590 dies was Gorringe bank (Serra and Ambar, 2002). Our results indicate three
591 new generation sites: seamounts Josephine, Lion and Ampère. These new
592 hotspots of formation coincide with convergence points of the major path-
593 ways described in Section 4.2.2, hence it is likely that the origin of Meddies
594 here is due to merging or “re-birth” of previous ones.

595 The latter possibility is exemplified in Figure 10: two weeks after a Meddy
596 ended its life on the stoss side of Josephine, a new Meddy is born on the
597 lee side of the same seamount. The original Meddy arrives from northeast,
598 shedding vorticity and salinity as it moves clockwise around the seamount due
599 to the local topographic β -effect. During the interaction with the seamount,
600 the Meddy signal is lost on day 06/24 as it is weakened beyond possible
601 detection. However, after one complete revolution the filaments of vorticity
602 are reinforced and reorganised into a new core that is able to detach from the
603 southern edge of Josephine. Note that the salinity in the core of the newly
604 formed Meddy (detected from the day 07/06 onwards) is lower than in the
605 previous one. Peculiar interactions of Meddies with seamounts have been
606 reported in literature (Richardson and Tychensky, 1998) and addressed by
607 idealised experiments (Cenedese, 2002). Figure 10 is merely illustrative and
608 the occurrence of merging and re-birth of Meddies will be carefully studied
609 in future work.

610 The more common pathways described here correspond to the ones pre-
611 viously known: near the eastern boundary Meddies will drift northwards or
612 northwestwards, while offshore Meddies tend to move westwards and south-
613 westwards (Richardson et al., 2000) reaching as far as the area south of the
614 Azores Islands and the Canary Basin (Richardson and Tychensky, 1998).
615 However, it is seen here that some Meddies will instead: i) translate south-
616 wards right after their formation, occasionally recirculating into the Gulf of
617 Cadiz, or ii) veer to west with a very small deviation to south, straight af-
618 ter formation in the Tagus Abyssal Plain or after an initial northwards drift

619 off Cape St. Vincent. Furthermore, the former Meddies will occasionally
620 spend some of their life-time near the Moroccan shelf, as first brought to
621 attention by the observations of Carton et al. (2002) and corroborated by
622 the recent sighting of a Meddy at about 12.5°W , 31.5°N (Ménèsguen et al.,
623 2012). These results show that cyclones tend to linger in the Gulf of Cadiz or
624 else (fewer ones) take a distinct path towards northwest. The presence of so
625 many cyclones in the Gulf of Cadiz is not entirely surprising and is supported
626 by observational evidence (Carton et al., 2002; Ambar et al., 2008). To our
627 knowledge, the possibility of having cyclones taking such a long northwest-
628 ward path since the Portimão Canyon is a new result.

629 In past literature, the full picture of Meddies pathways just described is
630 closest to that presented by Shapiro and Meschanov (1996) (their Figure 8)
631 when referring to the main spreading paths of MW in the Iberian Basin.

632 Based on observations from drifters, the rate of formation of Meddies is
633 expected to be between 8 – 12 per year (Richardson et al., 1989) and 15 – 20
634 per year (Bower et al., 1997). These two estimates are based on observations
635 of Meddies far from and in the vicinity the Iberian slope, respectively. By
636 adding the formation rates in the boxes containing the Portimão Canyon,
637 Cape St. Vincent and Estremadura Promontory, our results indicate that
638 between 8 and 18 Meddies are born every year along the southwestern Iberian
639 slope and survive for at least 90 and 15 days, respectively; these are in very
640 good agreement with observational estimates. In the region of Cape St.
641 Vincent alone, the upper rate of formation of $9.3 \text{ Meddies yr}^{-1}$ is very close
642 to the estimated 10 events per year based on data from drifters (Bower et al.,
643 1997; Ambar et al., 2008). However, the number of events detected in the
644 Estremadura Promontory is much lower than the estimate of 7 – 10 events
645 per year by Bower et al. (1997); Ambar et al. (2008). The latter could be due
646 to three reasons: i) the flow in this region is affected by its proximity to the
647 border of the domain, ii) the criteria for Meddies selection are too strict for
648 Meddies forming this far downstream, where the characteristics of MW are
649 expected to be more diluted, and iii) the Meddies' generation requires the
650 maintenance of a slope current (along the southwestern margin) that may
651 not be well reproduced in the model at such large distance from the Strait
652 of Gibraltar.

653 Among the Meddies living more than 15 days, cyclones account for 28–
654 31% of the population which comes very close to the 1:3 ratio (C:AC) antic-
655 ipated by Richardson et al. (2000).

656 Considering the whole domain of study, there are about 12 events per

657 year of Meddies living more than 90 days. Nearly 40% of these (4.5 Meddies
658 yr^{-1}) succeed in exiting the domain, carrying away a significant portion of
659 MW to the west and south, far into the North Atlantic.

660 Another important result from the present study is that long-lived Med-
661 dies correspond to no more than 40% of the total of Meddies generated (see
662 Table 4). The fate of short-lived Meddies should be investigated: is their dis-
663 appearance due to merging or destruction? Perhaps merging is a key process
664 for the survival of Meddies.

665 *6.2. Properties of Meddies*

666 The maximal time-mean radius of 50 – 60 km presented here are sup-
667 ported by records of floats. Some floats have described loops around 120 km
668 in diameter while trapped in Meddies far from the slope (Richardson and
669 Tychensky, 1998; Richardson et al., 2000).

670 Our results indicate that Meddies are about 50 km wide on average. No
671 major differences on the dynamical radius (where the velocity magnitude is
672 maximum, R_{vmax}) of anticyclones and cyclones were detected. The radius
673 computed here is slightly shorter than the dynamical radius and the dynam-
674 ical radius itself is shorter than the thermohaline core of the Meddies. For a
675 vortex with a Gaussian profile of radial velocity, the radius under the influ-
676 ence of the eddy’s velocity is approximately $R_0 \simeq \sqrt{2}R_{vmax}$ (Carton et al.,
677 2002).

678 If some Meddies are formed by separation of a frictional boundary layer
679 from the coast (D’Asaro, 1988), then the radius of young Meddies should be
680 about 10 km which is the estimated width of the anticyclonic shear zone of
681 the Mediterranean undercurrent (Bower et al., 1997). On the light of this
682 theory and of some observations (Bower et al., 1997; Serra and Ambar, 2002),
683 the minimum time-mean radii of 10 – 15 km computed here are acceptable
684 values.

685 Typically, the swirl velocities (model’s results) at the depth level of 600 m
686 are higher than at 1000 m. Anticyclones tend to rotate faster than cyclones
687 and peak azimuthal velocities are about 30 cm s^{-1} . Both results are in
688 agreement with values reported in past work (Richardson et al., 2000; Carton
689 et al., 2002; Serra and Ambar, 2002). However, records in Meddies with
690 dynamical radius smaller than 10 km have revealed velocities as high as 50
691 cm s^{-1} (Carton et al., 2010).

692 Past observations give reasons to believe that the swirl velocity tends to
693 decrease slightly as the distance to the point of origin increases: a behaviour

694 that is confirmed inhere at least at $z = 600$ m (Figure 5). Moreover, measure-
695 ments of distinct rotation rates, at different depths within recently formed
696 Meddies, suggest that the characteristic solid-body rotation of Meddies is
697 acquired as they evolve (Ambar et al., 2008). This is also supported by our
698 results where the largest differences in swirl velocity (at 600 m or 1000 m
699 depth) occur within the first 500 km since the point of origin.

700 Here, there is also an indication of distinct swirl velocities between Med-
701 dies formed in Cape St. Vincent or Portimão Canyon and Estremadura
702 Promontory which could be related to different generation mechanisms.

703 From measurements of floats inside Meddies in the open ocean, Richard-
704 son and Tychensky (1998) reported mean translation speeds of 2.5 ± 0.5 cm
705 s^{-1} , which is in good agreement with the mean value of ~ 3 cm s^{-1} obtained
706 here. The minimum value of 1.1 cm s^{-1} is also corroborated by past ob-
707 servations of Richardson et al. (1989). In spite of the limitation on speed
708 imposed by our tracking method (see Appendix A and Section 4.1.5), the
709 maximum translation speed detected here, 6.2 cm s^{-1} , agrees well with the
710 largest time-mean speeds of 6.4 cm s^{-1} recorded in observations (Richardson
711 et al., 2000).

712 Regarding temperature measurements, instantaneous observations in Med-
713 dies range from 11.4°C to 13°C (Serra and Ambar, 2002), while in cyclones
714 the values vary from 11°C to 12°C (Carton et al., 2002; Serra and Ambar,
715 2002; Ambar et al., 2008). Our results indicate time-mean values around
716 12°C in anticyclones and 11°C in cyclones. The latter are on average colder
717 than their counterparts as suggested by the earliest measurements in cyclones
718 by Richardson et al. (2000).

719 Also, our results show that anticyclones are slightly more saline than
720 cyclones. Note how the salinity is lower inside the cyclonic core in the two
721 examples of dipoles off Portimão Canyon and Estremadura Promontory (Fig-
722 ures 8 and 9). This is also supported by observations by Carton et al. (2002);
723 Ambar et al. (2008) who reported maximum values of $36.5 - 36.6$ psu for an-
724 ticyclones and $36.2 - 36.4$ psu for cyclones, in dipoles surveyed in the Gulf
725 of Cadiz.

726 The temperature and salinity anomalies presented here were computed
727 differently than what is usual in observational data. The extreme and mean
728 values produced here are smaller than typical values reported in observa-
729 tions. Nevertheless, the anomalies obtained are comparatively stronger in
730 anticyclones than in cyclones, as learned from in situ surveys as well.

731 Despite not being very common, some measurements within anticyclones

732 in the Gulf of Cadiz (Carton et al., 2010) show that these will occasionally
733 have a strong salinity anomaly below 1300 m. Such Meddies are unlikely
734 to be detected by the Meddy criteria used here and this may hinder the
735 detection of Meddies in the Gulf of Cadiz.

736 The eddy tracking results bear evidence that the dynamical signature of
737 cyclones is shallower than that of anticyclones. This brings further support to
738 the hypothesis that cyclones will often form above and to the side of an anti-
739 cyclone when the latter detaches from a cape or canyon, forming a baroclinic
740 dipole (Serra et al., 2002; Aiki and Yamagata, 2004). Likewise, the weaker
741 thermohaline anomalies of cyclones versus anticyclones favour the possibil-
742 ity that cyclones will gather water from the Upper Core, unlike anticyclones
743 whose MW content is largely provided by the Lower Core. Detailed hy-
744 drographic observations of dipoles are in agreement with this interpretation
745 (Carton et al., 2002).

746 Since more cyclones are found in the Gulf of Cadiz than elsewhere this
747 suggests that either the formation mechanisms of Meddies over there are more
748 prone to forming also cyclones (i.e. dipoles are formed), or (possibly “and”)
749 that cyclones survive longer there. The canyon formation mechanism implies
750 first the formation of a cyclone followed by the formation of an anticyclone
751 downstream; they are asymmetrical in a shallow-water model if the flow ini-
752 tially has potential vorticity $(\omega_c + f)/(h + \delta h) = (\omega_0 + f)/h = (\omega_a + f)/(h - \delta h)$
753 or possibly the ω_c and ω_a (relative vorticity of the cyclone and anticyclone,
754 respectively) can be due to different mechanisms such as topography for the
755 first one and curvature for the second one; where f is the Coriolis parameter,
756 ω_0 is the initial relative vorticity of the MW undercurrent, h is its initial
757 thickness and δh is its thickness variation due to topography.

758 In sigma-coordinate models, the realism of topography is a compromise
759 between the desired steepness of the terrain and a spurious pressure gradient
760 force generated over very steep slopes. To reduce the latter effect, a substan-
761 tial amount of smoothing is required unless the resolution is very high. In our
762 case, even with a 3 km resolution, the topography had to be smoothed. Al-
763 though the relevant details of the topography such as promontories, canyons
764 and seamounts are preserved here, future simulations should consider higher
765 resolutions (smaller than 2 km). An improved topography (steepness) and
766 higher vertical resolutions may significantly increase the realism of the out-
767 flow and of the Meddies’ generation ultimately.

768 7. Conclusions

769 In the present work, the Mediterranean Outflow was simulated at high
770 resolution, over a period of 20 years. The simulation included atmospheric
771 forcing and the boundary conditions at the Strait of Gibraltar were taken
772 from a previous numerical study which focused on Mediterranean–Atlantic
773 exchanges. The output velocity fields were searched for eddies at two depth
774 levels: 600 and 1000 m. The eddies were tracked throughout their life-times
775 and those containing MW (Meddies) were identified using a criteria that
776 takes into account the salinity anomaly vertically-averaged between 600 and
777 1300 m. The formation of Meddies was recurrent and the domain was large
778 enough to allow the structures to freely evolve, following their natural fate.
779 The large number of records ensures the statistical significance of the results
780 gathered here. Nevertheless, the population of Meddies varied depending on
781 the thresholds used for the Meddies’ life-time and salinity anomaly.

782 For Meddies living a minimum of 15 days and having a minimum salinity
783 anomaly of 0.12 psu, the formation rates along the southwestern Iberian slope
784 are of 16–18 Meddies per year. Considering the whole domain of study, 28–
785 31% of the Meddies within this dataset are cyclones. Among the datasets
786 studied here, this one exhibits the slope’s formation rate and fraction of
787 cyclones that are closer to previous estimates based on observational records.

788 Some robust Meddies form far from the slope, in the Tagus Abyssal Plain
789 and Horseshoe seamounts. These events are likely to be due to merging or
790 re-birth of previously existing Meddies as illustrated above. In the future,
791 such events will be studied in more detail.

792 There is an abundance of cyclones (anticyclones) upstream (downstream)
793 of Cape St. Vincent which is most certainly an indicator of different under-
794 lying dynamics. However, it is not clear whether this asymmetry is due to
795 the generation process itself or the evolution of each type of structure. The
796 longest-lived Meddies propagate northwestward: while anticyclones depart
797 from the western slope, cyclones depart from the southern Iberian slope.
798 Most of the anticyclones will also veer southwestwards but the cyclones will
799 either move northwestwards or recirculate in the Gulf of Cadiz. Three cy-
800 clones (much less than anticyclones) that live longer than 90 days and with
801 a salinity anomaly above 0.3 psu can only be seen off Portimão Canyon at
802 $z = 1000$ m, probably because the dynamical core lies deeper in these Med-
803 dies. Larger survival rates of cyclones near Portimão Canyon may be due
804 to trapping by topography, to the recirculation gyre, or to re-intensification

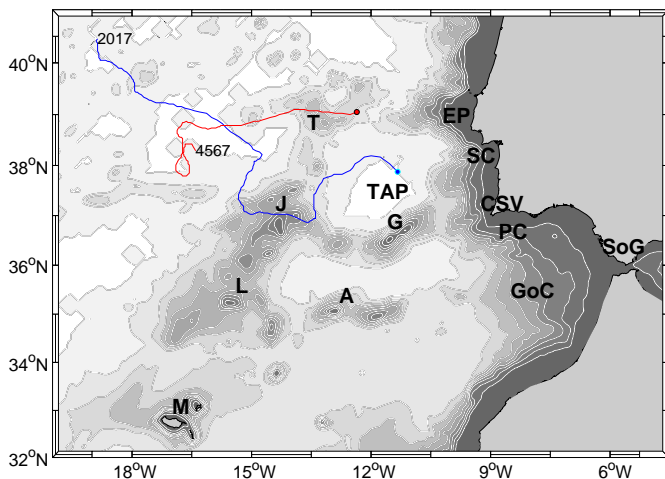


Figure 1: Domain of study with bathymetry shown in gray scale at regular intervals of 500 m. Strait of Gibraltar (SoG), Gulf of Cadiz (GoC), Madeira Island (M), Tore Seamount (T) and Tagus Abyssal Plain (TAP). Southwestern Iberian slope: Portimão Canyon (PC), Cape St. Vincent (CSV), Setubal Canyon (SC), Estremadura Promontory (EP). Horseshoe Seamounts: Josephine (J), Lion (L), Ampère (A) and Goringe bank (G). The red (anticyclone) and blue (cyclone) lines correspond to examples of Meddies and the circles mark the Meddies' birthplace (see Figure B.11).

805 processes and this remains an open question.

806 In future work, the results from realistic numerical simulations will be
 807 used to study in detail the processes of formation, interaction and disruption
 808 of Meddies in the main locations identified inhere.

809 Acknowledgments

810 The authors would like to thank F. Nencioli for providing the source code
 811 of his automatic eddy detection algorithm. This study had the support of
 812 Fundação para a Ciência e Tecnologia (FCT) through the projects MedEx
 813 (MARIN-ERA/MAR/0002/2008) and Sflux (PTDC/MAR/100677/2008). A.
 814 C. Barbosa Aguiar was funded through the grant SFRH/BPD/64099/2009
 815 by the FCT. X. Carton acknowledges the support of SHOM for the SEMANE
 816 programme.

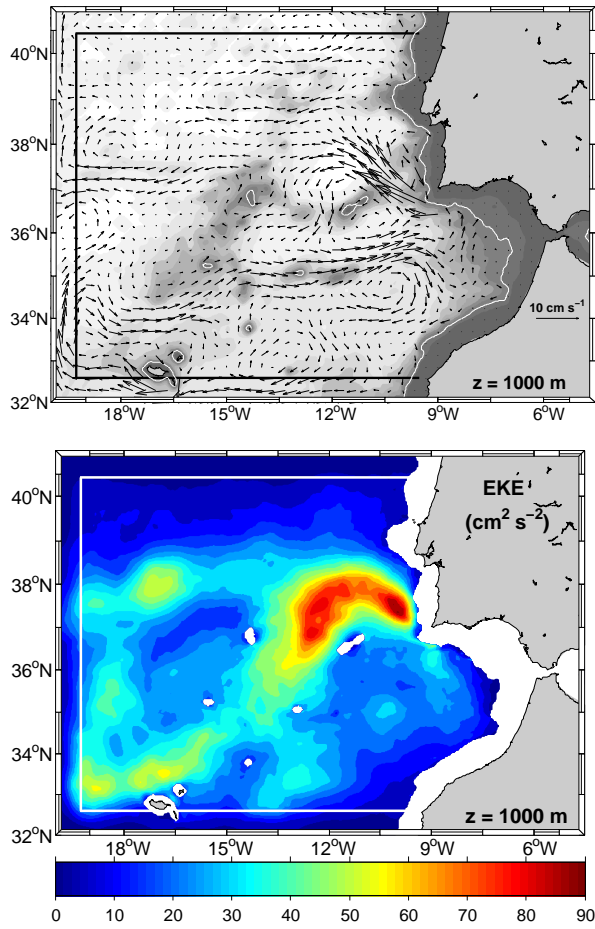


Figure 2: Top: Mean velocity field (20-years) with vectors represented at each 10 grid-points and the 1000 m isobath in white. Bottom: Eddy Kinetic Energy (20-years). The straight lines (black/white) give the approximate limits of the sponge band (see Section 2.2).

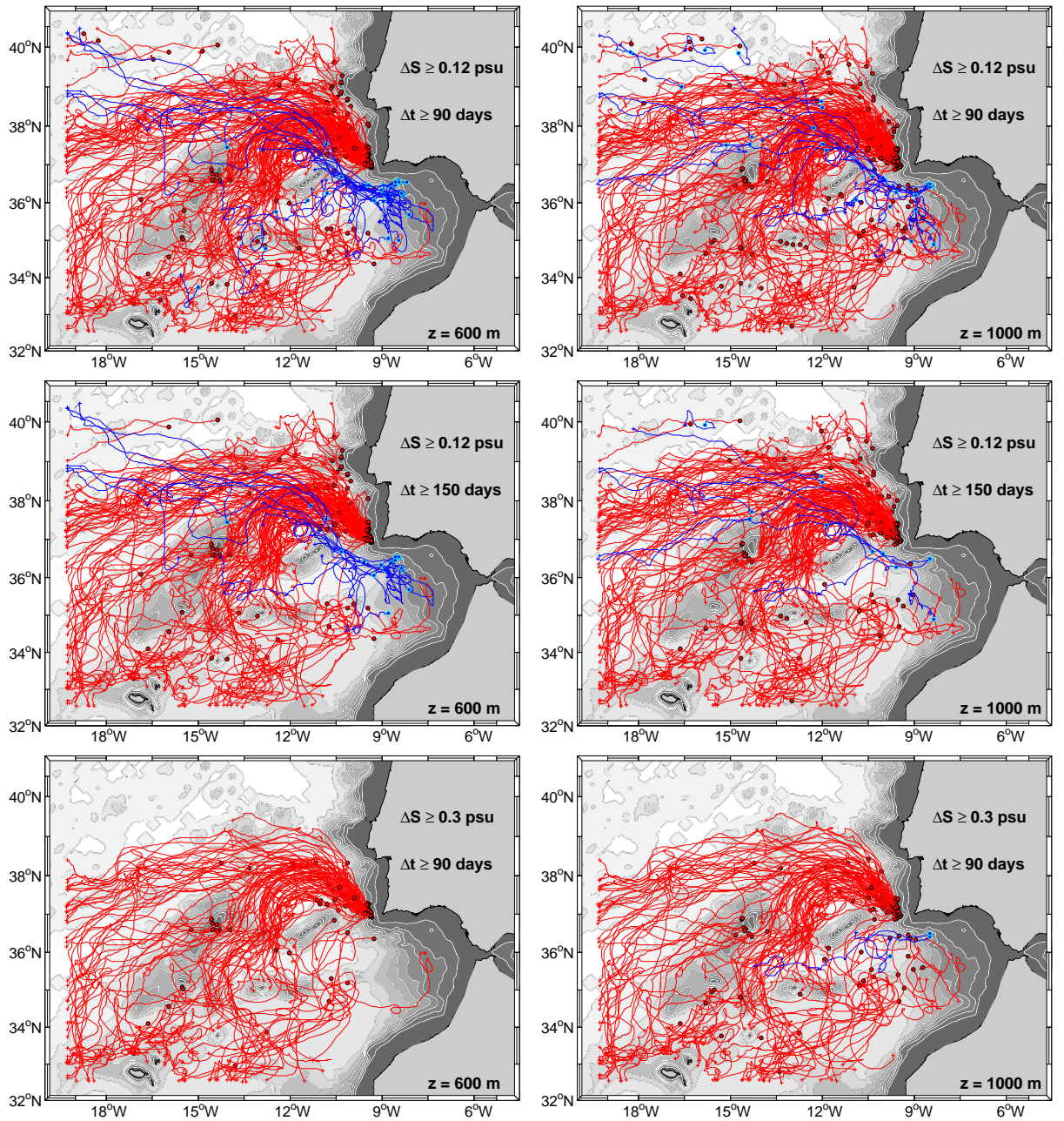


Figure 3: Trajectories of Meddies born during 20 yrs of simulation in the whole domain ($r = 18$ km): comparison of trajectories for different thresholds of eddy life-time Δt and minimum salinity anomaly ΔS (mean over at least half the life-time), at the respective z -level. Red (blue) lines correspond to anticyclones (cyclones) while circles in different colour mark their “birth”. The bathymetry is shown in gray scale at regular intervals of 500 m.

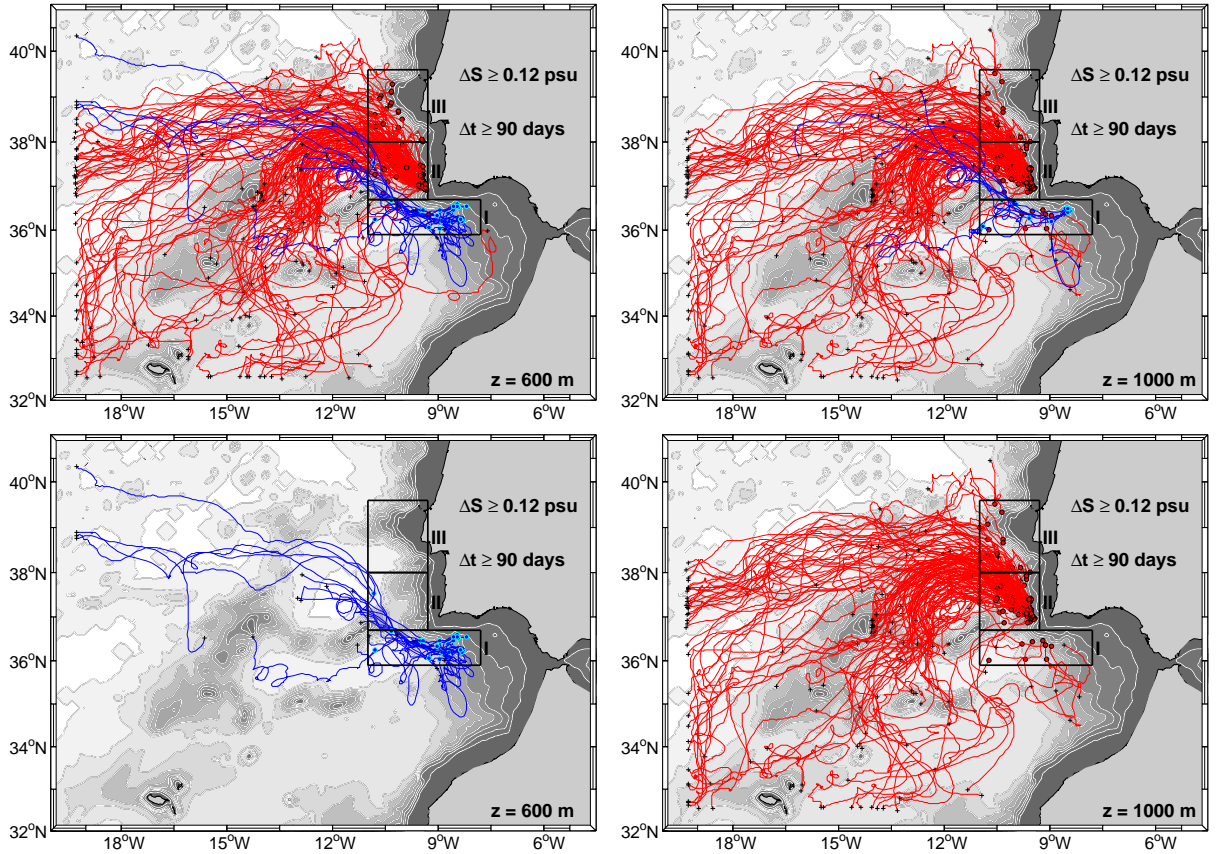


Figure 4: Trajectories of Meddies born within boxes I, II and III during 20 yrs of simulation. This is a subset of the whole domain population ($\Delta S \geq 0.12$ psu and $\Delta t \geq 90$ days) shown in Figure 3 (top). Bottom-left: only cyclones tracked at $z = 600$ m. Bottom-right: only anticyclones tracked at $z = 1000$ m. Red (blue) lines correspond to anticyclones (cyclones), while circles in different colour mark their “birth” and black crosses mark their “death”. The boxes correspond to the three slope regions of Meddies’ formation (see Section 4.2.1). The bathymetry is shown in gray scale at regular intervals of 500 m.

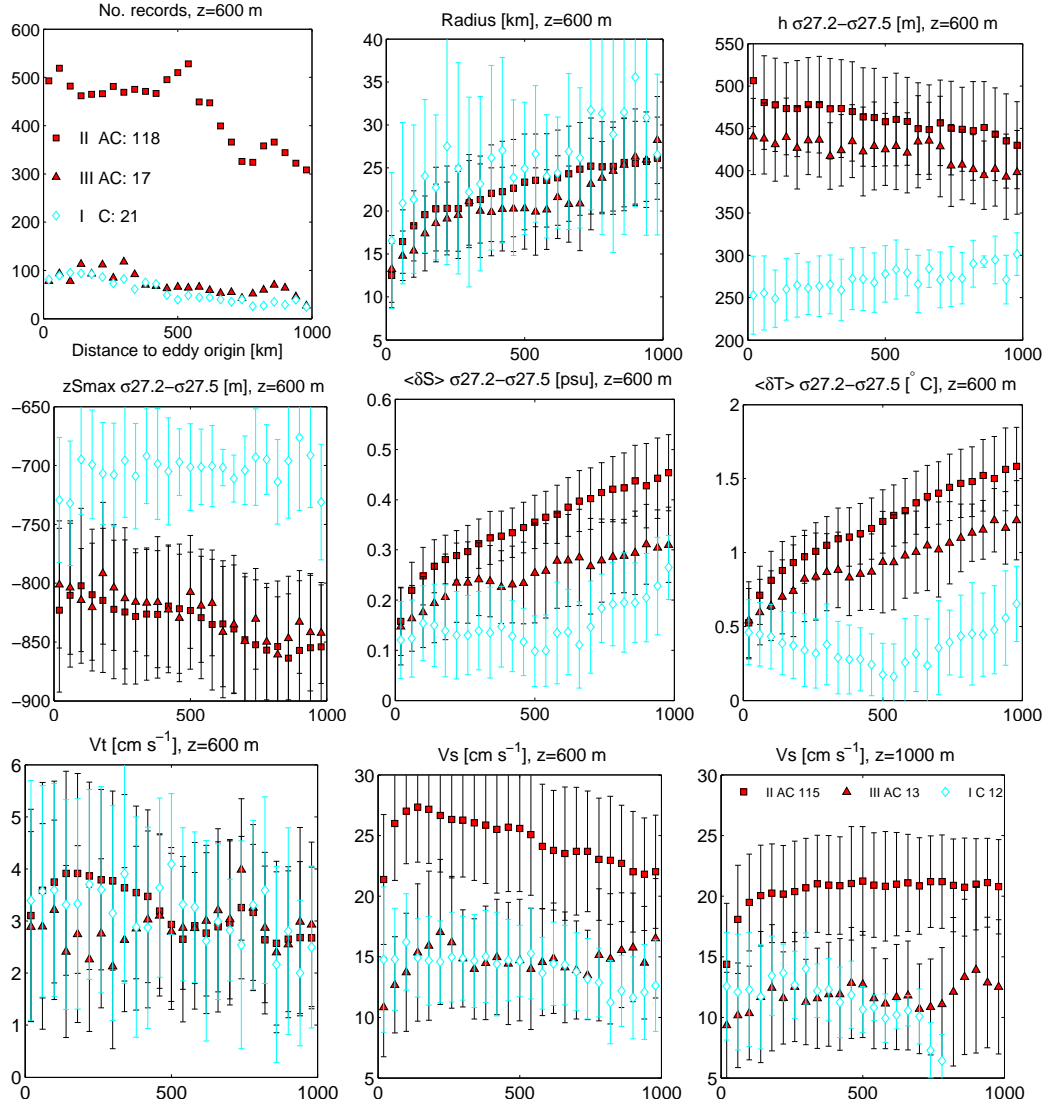


Figure 5: Properties of Meddies born in boxes I, II and III ($\Delta S \geq 0.12$ psu and $\Delta t \geq 90$ days, Figure 4) as a function of curvilinear distance to origin, for eddy tracking at $z = 600$ m. In the first chart is shown the number of records available in each case and the numbers in the legend correspond to the total of Meddies born in each box. In the remaining charts are represented the mean values (markers) and the standard deviation (errorbars) computed with all the records collected at each 40 km of distance (see Section 4.2.3 for details). Swirl velocity at $z = 1000$ m is shown in the last graph, with the total of Meddies per box in the legend.

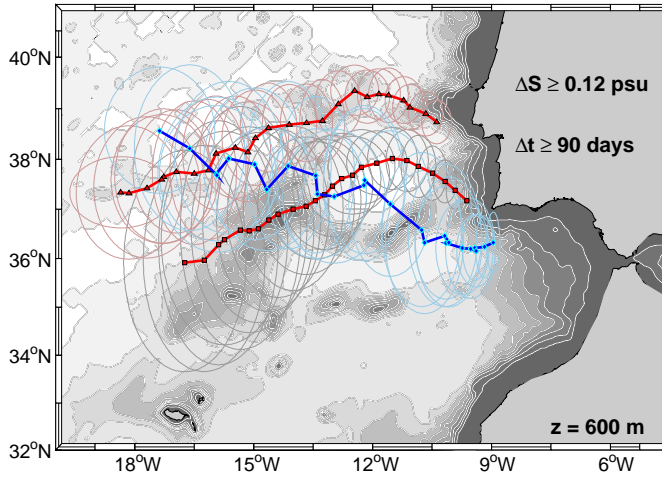


Figure 6: Mean trajectories of Meddies born in boxes I, II, and III, corresponding to the dataset analysed in Figure 5 and shown in Figure 4. The standard deviation on longitude and latitude is represented by the size of the horizontal and vertical axis of each ellipse. The ellipses corresponding to data from box I, II and III are coloured in light blue, gray and pink respectively.

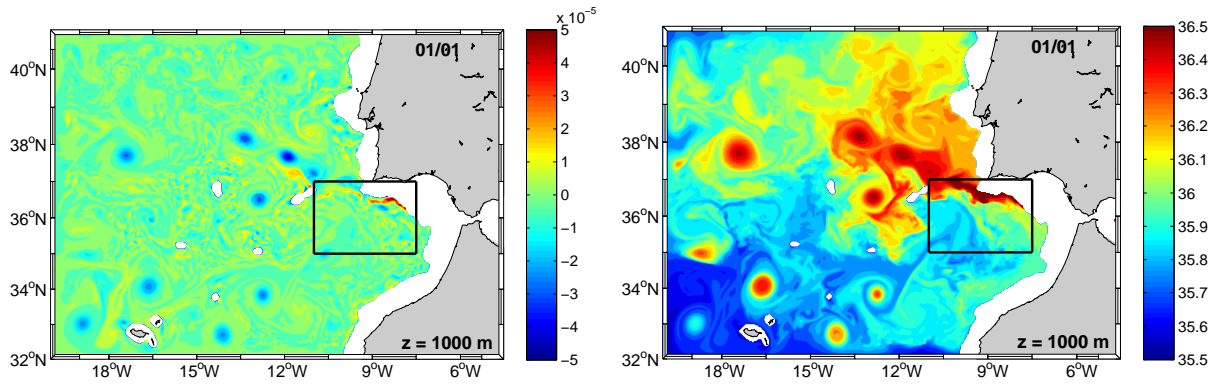


Figure 7: Snapshots of vorticity (s^{-1}) and salinity (psu) fields at $z = 1000$ m on the left and right, respectively. See Figure 8 for a time-sequence of the area within the black box.

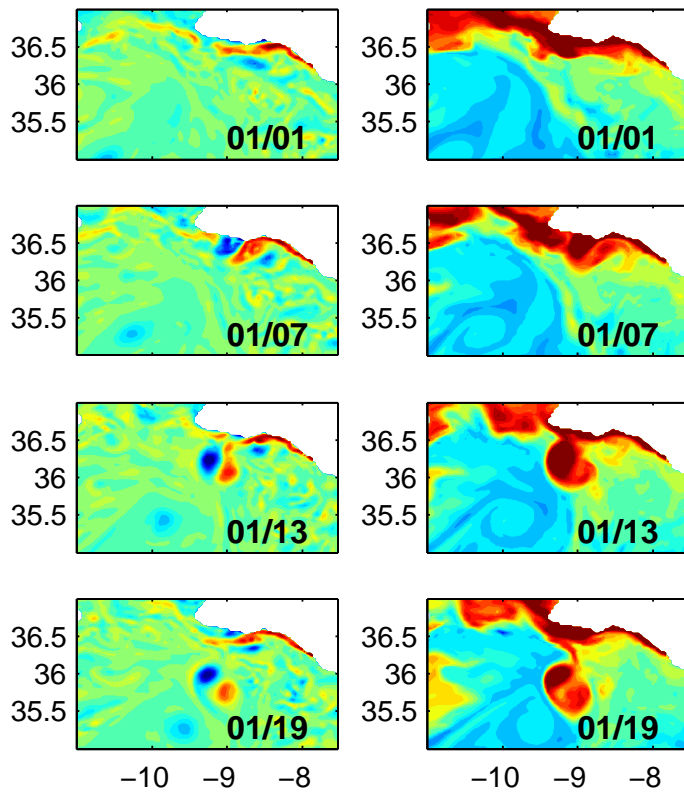


Figure 8: Time sequence of vorticity and salinity fields during the generation of a dipole off Portimão Canyon (same colourscale and depth as in Figure 7). Time is given in each frame as mm/dd : mm =month, dd =day.

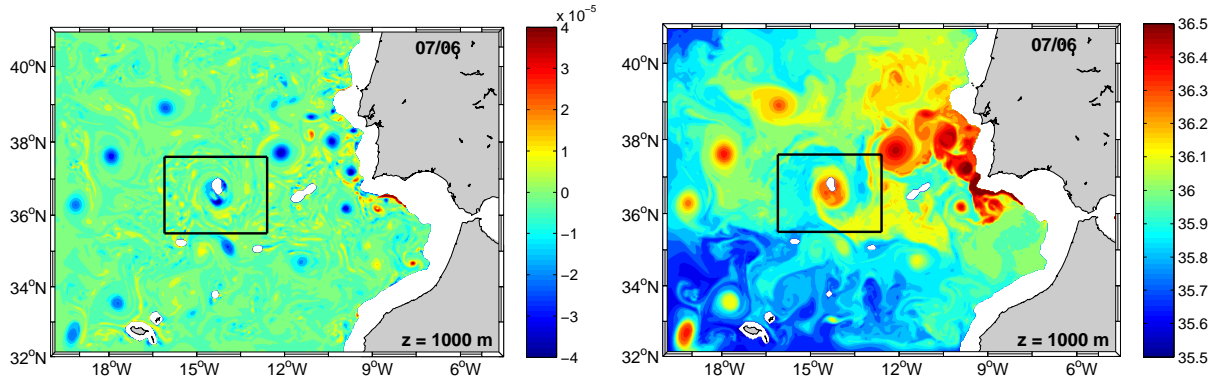


Figure 9: Snapshots of vorticity (s^{-1}) and salinity (psu) fields at $z = 1000$ m on the left and right, respectively. Note the formation of a small dipole at about $(11^{\circ}W, 38.5^{\circ}N)$. See Figure 10 for a time-sequence of the area within the black box.

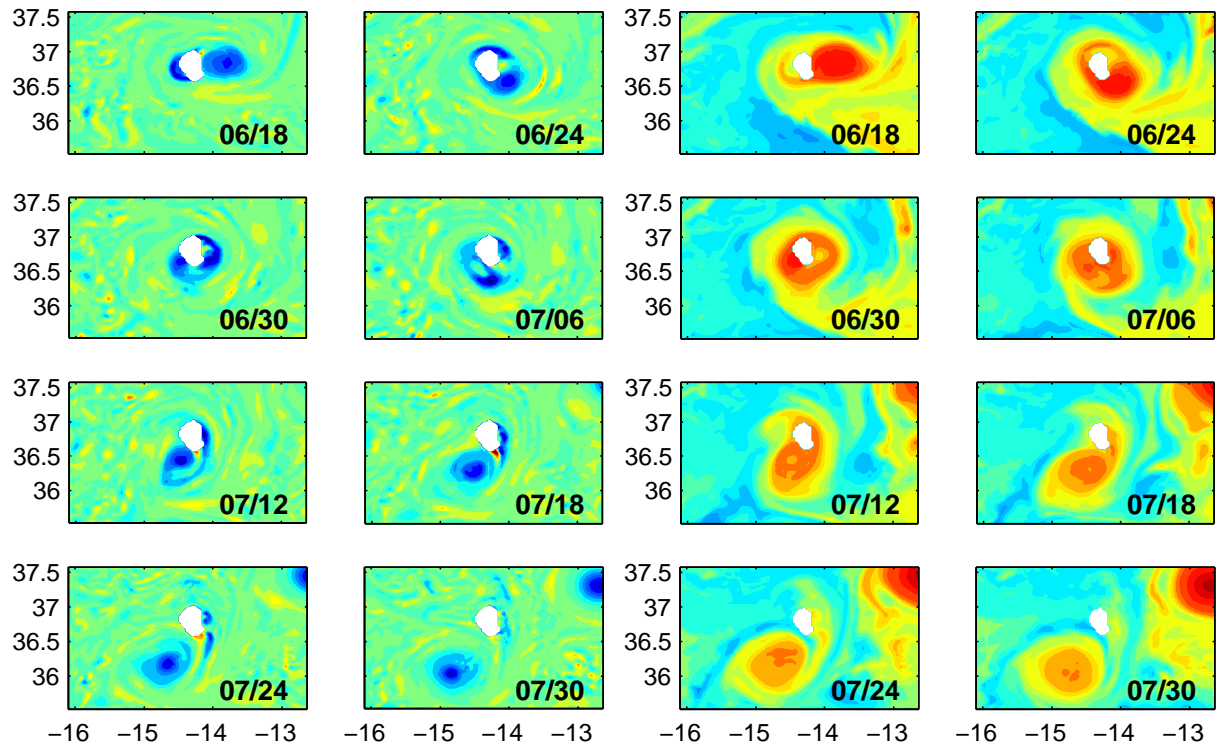


Figure 10: Time sequence of vorticity and salinity fields depicting the “death” (06/24) and “birth” (07/06) of a Meddy at Josephine seamount (same colourscale and depth as in Figure 9). Time is given in each frame as mm/dd : mm =month, dd =day.

$\Delta S \geq$		0.12	0.2	0.3
$z = 600$ m	Total units yr ⁻¹	11	8.1	5.2
$r = 18$ km	% C	14	4	0
$z = 1000$ m	Total units yr ⁻¹	12.2	8.9	6
$r = 18$ km	% C	12	5	3
$z = 600$ m	Total units yr ⁻¹	10.5	7.6	5
$r = 36$ km	% C	14	2	0
$z = 1000$ m	Total units yr ⁻¹	11.4	8.4	5.5
$r = 36$ km	% C	13	5	3

Table 1: Time-mean Rates of Formation in the Whole Domain. For datasets of Meddies with different ΔS [psu] thresholds and $\Delta t \geq 90$ days (see Figure 3 top and bottom). Total units yr⁻¹: rates of formation of anticyclones and cyclones altogether; % C, percentage of cyclones.

$\Delta S \geq$		0.12	0.2	0.3
$z = 600$ m	Total units yr ⁻¹	4.3	3.3	2.8
$r = 18$ km	% Meddies	39	41	54
$z = 1000$ m	Total units yr ⁻¹	4.5	3.6	3
$r = 18$ km	% Meddies	37	41	50
$z = 600$ m	Total units yr ⁻¹	4.4	3.4	2.9
$r = 36$ km	% Meddies	42	45	57
$z = 1000$ m	Total units yr ⁻¹	4.4	3.6	2.9
$r = 36$ km	% Meddies	39	43	52

Table 2: Rates of Exit to the North Atlantic. For datasets of Meddies with different ΔS [psu] thresholds and $\Delta t \geq 90$ days (see Figure 3 top and bottom). Total units yr⁻¹: rates of exit of anticyclones and cyclones altogether; % Meddies, percentage of Meddies formed that succeed in exiting the domain.

	Δt (days)	Δd (km)	R (km)	V_s (cm s ⁻¹)	V_t (cm s ⁻¹)	S (psu)	δS (psu)	T (°C)	δT (°C)
190 AC, $z = 600$ m									
min	90	105	10	4	1.1	35.9	0.10	10.7	0.51
max	1011	1987	64	32	6.2	36.5	0.54	12.8	2.22
mean	321	805	23	21	3.1	36.3	0.31	12.2	1.34
31 C, $z = 600$ m									
min	90	153	13	8	1.7	35.8	0.1	10.2	0.09
max	492	1253	50	23	6	36.3	0.29	11.6	0.72
mean	207	549	27	13	3.2	36.1	0.17	11.1	0.35
216 AC, $z = 1000$ m									
min	90	121	11	3	1.5	35.9	0.11	10.7	0.41
max	1011	1969	48	28	6.1	36.5	0.57	12.8	2.44
mean	291	728	24	16	3.1	36.3	0.31	12.1	1.31
28 C, $z = 1000$ m									
min	93	118	15	4	1.5	36	0.09	10.5	0.11
max	378	795	47	16	5.2	36.3	0.32	11.8	0.94
mean	165	417	24	10	3	36.2	0.17	11.1	0.38

Table 3: Properties of Meddies in the Whole Domain, $\Delta t \geq 90$ days and $\Delta S \geq 0.12$ psu (Figure 3 top). AC, anticyclones; C, cyclones; Δt , eddy life-time; Δd , distance travelled; R , radius (given by the median radius of each eddy); V_s and V_t are respectively the swirl and translation velocity; S , δS , T and δT are respectively the salinity, salinity anomaly, temperature and temperature anomaly depth-averaged between $z = 600$ m and $z = 1300$ m, along the vertical axis of the eddy “centre” detected at $z = 600$ m or $z = 1000$ m. V_s , V_t , S , δS , T and δT correspond to time-averaged values along an eddy’s trajectory.

		$\Delta t \geq 15$ days				$\Delta t \geq 90$ days			
		I	II	III	WD	I	II	III	WD
$z = 600$ m	Total units yr ⁻¹	5.5	9.2	1.3	29	1.2	6	0.9	11
$r = 18$ km	% C	84	4	4	31	91	0.8	0	14
$z = 1000$ m	Total units yr ⁻¹	7.2	9.3	1.4	40	1	5.8	0.7	12
$r = 18$ km	% C	61	3	4	28	57	0	0	12
$z = 600$ m	Total units yr ⁻¹	4.8	9	1.4	26	1	5.9	0.9	10.5
$r = 36$ km	% C	83	4	4	30	90	0.9	0	14
$z = 1000$ m	Total units yr ⁻¹	6.6	9	1.2	36	1.3	5.8	0.5	11.4
$r = 36$ km	% C	63	2	0	28	48	0	0	13

Table 4: Rates of Formation of Meddies per Region, $\Delta S \geq 0.12$ psu. Total units yr⁻¹: rates of formation of anticyclones and cyclones altogether; % C, percentage of cyclones born within each region; WD, Whole Domain.

817 **Appendix A. Eddy Tracking**

818 In order to identify vortices in the horizontal velocity fields, the algorithm
819 developed by Nencioli et al. (2010) starts by locating their centres. To do so,
820 the algorithm searches for points where the following constraints are verified.

- 821 1. In the zonal direction, it searches for a pair of grid-points such that
822 the meridional velocity i) reverses its sign and ii) has increasing magni-
823 tude within a grid-points to each side of the pair. For the points thus
824 selected, the same procedure is applied along the meridional direction
825 for the zonal velocity.
- 826 2. The algorithm then searches for a local minimum of velocity in a square
827 of side $2b \times 2b$ centred on one of the points identified in step 1. That
828 local minimum is considered a candidate for the centre assuming it
829 passes a similar check.
- 830 3. To discard non-eddy structures that pass the previous constraints, the
831 velocity vectors are checked to exhibit a constant sense of rotation
832 around the candidate eddy's centre.

833 Once identified, the coordinates of the eddy's centre and boundary are recorded
834 and the eddy can be tracked along consecutive velocity fields. For further
835 details see Nencioli et al. (2010).

836 After comparing the eddies' centres obtained with different values of
837 search parameters (not shown), we decided to use $a = 4$ and $b = 3$ which
838 provided the most successful detection. This choice sets the radius of the
839 smallest detectable vortices to 9–12 km, given the model's spatial-resolution
840 of 3 km.

841 An eddy's boundary was defined as the outermost closed streamline,
842 within a specified number of grid-points ($nrad = 8$) from the eddy's cen-
843 tre (in a first instance), where the velocity magnitude was still increasing
844 in the radial direction. This area was enlarged whenever necessary to ac-
845 commodate for larger eddies. The radius of the eddy was estimated as the
846 mean distance from every boundary-point to the centre of the eddy. There
847 is no optimal criterion to determine the dimensions of an eddy automatically
848 detected and, while the method adopted here may lead to a slight underes-
849 timation of the radius (see Nencioli et al., 2010, Figure 6), it is guaranteed
850 to return the dimensions of closed structures.

851 The trajectories are retrieved by following each eddy across consecutive
852 velocity fields: two eddies identified separately at t and $t + 1$ are considered

853 to be the same structure if they have the same vorticity sign and if the
854 distance between the two is smaller or equal to $r = \{18, 36\}$ km (Nencioli
855 et al. (2010), Section 3c). This algorithm is able to track eddies across
856 non-consecutive velocity fields, which is an advantage since these eddies will
857 often suffer strong distortions and lose their dynamical signature during
858 interactions with neighbouring eddies or topography. However, if the eddy
859 does not recover a coherent signal after two consecutive maps, its tracking
860 ends.

861 In addition, a minimum eddy life-time of $\Delta t = N \cdot \delta t_{out} \geq 15$ days
862 was imposed by selecting only the trajectories with a minimum of 5 points
863 ($N \geq 5$).

864 After running the eddy tracking algorithm over the 20 years of numerical
865 data, a total of 6030 and 6835 (5767 and 6691) eddies were identified at
866 $z = 600$ m and $z = 1000$ m, respectively, for $r = 18$ km ($r = 36$ km).

867 The translation speed of the eddies detected was limited to 7 or 14 cm
868 s^{-1} when using $r = 18$ km or $r = 36$ km, respectively. While it is desirable
869 to allow for maximum speeds closer to the observed maxima of 17 cm s^{-1}
870 (Richardson et al., 2000), this incurred a higher risk of merging the trajecto-
871 ries of two independent eddies of the same vorticity sign, if: 1. one vanished
872 and 2. the other formed within the same area and at about the same time.
873 Some results are presented here for both values of parameter r , but most of
874 the results discussed focus on the dataset of eddies obtained with $r = 18$ km.

875 Appendix B. Selection of Meddies

876 In order to check whether an eddy should be classified as a Meddy or
877 not, we computed the salinity anomaly profile corresponding to every point
878 of its trajectory: $\Delta S^*(t, z)$, $t = \{1, \dots, N\}$, as illustrated in Figure B.11
879 (top). This anomaly was computed with respect to the local monthly values
880 of salinity time-averaged over the 20 years; in other words, this anomaly
881 corresponded to the salinity profile at the eddy centre minus the local 20-
882 year mean salinity.

883 Then, a characteristic salinity anomaly at MW levels was computed for
884 each eddy: by depth-averaging $\Delta S^*(t, z)$ over z -levels within the upper $600 \leq$
885 $z < 1000$ m (UMW) and deeper $1000 \leq z < 1300$ m (DMW) layers.

886 In the end, an eddy would be classified as a Meddy only if its depth-
887 averaged salinity anomaly was above a threshold value ΔS during a fraction
888 of its life-time $\gamma = (n_{UMW} + n_{DMW}) / (2N)$; here N is the total of points in

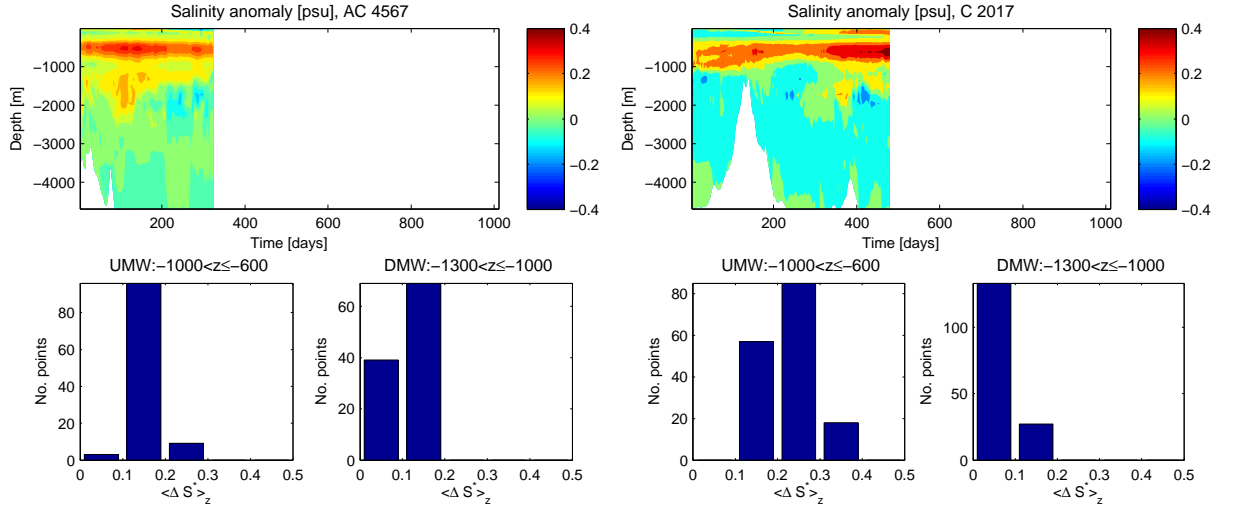


Figure B.11: Top: depth-profiles of the salinity anomaly recorded for an AC (left) and a C (right), both tracked at $z = 600$ m along the trajectories shown in Figure 1. Bottom: histograms of the depth-averaged salinity anomaly computed over the Upper or Deeper Mediterranean Water levels (UMW, DMW), at each point (instant of time) of the eddy's trajectory; if at least half of the points exhibit $\langle \Delta S \rangle_z$ above a specified threshold, then the eddy is classified as a Meddy (see Appendix B for more details).

889 the trajectory, n_{UMW} is the number of points with $\langle \Delta S^* \rangle_{UMW}(t) \geq \Delta S$ and
 890 likewise for n_{DMW} (see histograms in Figure B.11 bottom).

891 When first plotting all trajectories of Meddies, some boundary effects
 892 were evidenced by Meddies recirculating along the boundaries due to the
 893 effect of the sponge layers on the eddy vorticity. Therefore, all the records of
 894 Meddies within approximately 65 km to the boundaries were discarded before
 895 performing the statistics below. That distance corresponds to the sponge's
 896 width plus 15 km, permitting mean-sized Meddies (radius below 30 km, see
 897 Table 3) to penetrate at most 30% of the sponge layer.

898 References

- 899 Aiki, H., Yamagata, T., 2004. A numerical study on the succes-
 900 sive formation of Meddy-like lenses. J. Geophys. Res. 109, C06020.
 901 doi:10.1029/2003JC001952.
- 902 Ambar, I., 1983. A shallow core of Mediterranean Water off western Portugal.
 903 Deep-Sea Res. 30, 677–680.

- 904 Ambar, I., Serra, N., Neves, F., Ferreira, T., 2008. Observations of the
905 Mediterranean Undercurrent and eddies in the Gulf of Cadiz during 2001.
906 *J. Marine Sys.* 71, 195–220.
- 907 Antonov, J., Locarnini, R., Boyer, T., Mishonov, A., Garcia, H., 2006. World
908 Ocean Atlas 2005 Volume 2: Salinity. NOAA Atlas NESDIS 62, U.S.
909 Government Printing Office, Washington, D.C.
- 910 Barbosa Aguiar, A.C., Peliz, A.J., Cordeiro Pires, A., Le Cann, B., 2011.
911 Zonal structure of the mean flow and eddies in the Azores Current system.
912 *J. Geophys. Res.* 116. doi:10.1029/2010JC006538.
- 913 Bower, A., Serra, N., Ambar, I., 2002. Structure of the Mediter-
914 ranean undercurrent and Mediterranean water spreading around the
915 southwestern Iberian Peninsula. *J. Geophys. Res.* 107, C10,3161.
916 doi:10.1029/2001JC001007.
- 917 Bower, A.S., Armi, L., Ambar, I., 1997. Lagrangian observations of
918 Meddy formation during a Mediterranean undercurrent seeding experi-
919 ment. *J. Physical Oceanogr.* 27, 2545–2575.
- 920 Carton, X., Chérubin, L., Paillet, J., Morel, Y., Serpette, A., Le Cann, B.,
921 2002. Meddy coupling with a deep cyclone in the Gulf of Cadiz. *J. Ma-
922 rine Sys.* 32, 13–42.
- 923 Carton, X., Daniault, N., Alves, J., Chérubin, L., Ambar, I., 2010.
924 Meddy dynamics and interaction with neighboring eddies southwest of
925 Portugal: Observations and modeling. *J. Geophys. Res.* 115, C06017.
926 doi:10.1029/2009JC005646.
- 927 Cenedese, C., 2002. Laboratory experiments on mesoscale vor-
928 tices colliding with a seamount. *J. Geophys. Res.* 107, C6–3053.
929 doi:10.1029/2000JC000599.
- 930 Chérubin, L., Carton, X., Dritschel, D., 2007. Vortex dipole formation by
931 baroclinic instability of boundary currents. *J. Physical Oceanogr.* 37, 1661–
932 1677.
- 933 Chérubin, L., Carton, X., Paillet, J., Morel, Y., Serpette, A., 2000. Instability
934 of the Mediterranean water undercurrents southwest of Portugal: effects
935 of baroclinicity and of topography. *Oceanologica Acta* 23, 551–573.

- 936 da Silva, A., Young, C.C., Levitus, S., 1994. Atlas of Surface Marine Data
937 1994, Volume 1: Algorithms and Procedures. NOAA Atlas NESDIS 6.
938 U.S. Department of Commerce. Washington, D.C.
- 939 D’Asaro, E.A., 1988. Generation of submesoscale vortices: A new mecha-
940 nism. *J. Geophys. Res.* 93, 6685–6693.
- 941 Demidov, A.N., Filyushkin, B.N., Kozhelupova, N.G., 2012. Detection of
942 Mediterranean Lenses in the Atlantic Ocean by Profilers of the Argo
943 Project. *Oceanology* 52, 171–180. doi:10.1134/S0001437012020038.
- 944 Dong, C., Lin, X., Liu, Y., Nencioli, F., Guani, Y., Chao, Y.,
945 Dickey, T., McWilliams, J., 2012. Three-Dimensional Eddy Analy-
946 sis in the Southern California Bight. *J. Geophys. Res.* 117, C00H14.
947 doi:10.1029/2011JC007354.
- 948 Drillet, Y., Bourdallé-Badie, R., Siefridt, L., Le Provost, C., 2005. Meddies in
949 the Mercator North Atlantic and Mediterranean Sea eddy-resolving model.
950 *J. Geophys. Res.* 110, C03016. doi:10.1029/2003JC002170.
- 951 Duarte, R., Carton, X., Capet, X., Cherubin, L.M., 2011. Trapped instability
952 and vortex formation by an unstable coastal current. *Reg. Chaotic Dyn.*
953 16, 577–601.
- 954 Hedström, K.S., 2009. Technical Manual for a Coupled Sea-Ice/Ocean Circu-
955 lation Model (Version 3). Technical report. Artic Region Supercomputing
956 Center, University of Alaska Fairbanks.
- 957 Jungclauss, J., Mellor, G., 2000. A three-dimensional model study of the
958 Mediterranean outflow. *J. Marine Sys.* 24, 41–66.
- 959 Kida, S., Price, J.F., Jiayan, Y., 2008. The Upper-Oceanic Response to
960 Overflows: A Mechanism for the Azores Current. *J. Physical Oceanogr.*
961 38, 880–895. doi:10.1175/2007JPO3750.1.
- 962 Lamas, L., Peliz, A., Ambar, I., Barbosa Aguiar, A., Maximenko, N., Teles-
963 Machado, A., 2010. Evidence of time-mean cyclonic cell southwest of
964 Iberian Peninsula: The Mediterranean Outflow-driven β -plume? *Geo-
965 phys. Res. Lett.* 37. doi:10.1029/2010gl043339.

- 966 Large, W., McWilliams, J., Doney, S., 1994. Oceanic vertical mixing: A Re-
967 view and model with a nonlocal boundary layer parameterization. *Reviews*
968 *of Geophysics* 32, 363–403.
- 969 Locarnini, R., Mishonov, A., Antonov, J., Boyer, T., Garcia, H., 2006. World
970 Ocean Atlas 2005 Volume 1: Temperature. NOAA Atlas NESDIS 61, U.S.
971 Government Printing Office, Washington, D.C.
- 972 Marchesiello, P., Debreu, L., Couvelard, X., 2009. Spurious diapycnal mixing
973 in terrain-following coordinate models: The problem and a solution. *Ocean*
974 *Modelling* 26, 156 – 169. doi:10.1016/j.ocemod.2008.09.004.
- 975 Marchesiello, P., McWilliams, J.C., Shchepetkin, A.F., 2001. Open boundary
976 conditions for long-term integration of regional oceanic models. *Ocean*
977 *Modelling* 3, 1–20.
- 978 Ménesguen, C., Hua, B.L., Carton, X., Klingelhoefer, F., Schnurle, P., Re-
979 ichert, C., 2012. Arms winding around a meddy seen in seismic reflection
980 data close to the Morocco coastline. *Geophys. Res. Lett.* 39, L05604, 6pp.
981 doi:10.1029/2011GL050798.
- 982 Nencioli, F., Dong, C., Dickey, T., Washburn, L., McWilliams, J., 2010.
983 A vector geometry based eddy detection algorithm and its application to
984 high-resolution numerical model products and high-frequency radar surface
985 velocities in the southern California Bight. *J. Atmos. Oceanic Tech.* 27,
986 564–579. doi:10.11175/2009JTECHO725.1.
- 987 Paillet, J., Le Cann, B., Serpette, A., Morel, Y., Carton, X., 1999. Real-
988 time tracking of a Galician meddy. *Geophys. Res. Lett.* 26, 1877–1880.
989 doi:10.1029/2007JC004159.
- 990 Peliz, A., Boutov, D., Cardoso, R., Delgado, J., Soares, P., 2013. The gulf
991 of cadiz-alboran sea sub-basin: Model setup, exchange and seasonal vari-
992 ability. *Ocean Modelling* 61, 49–67. doi:10.1016/j.ocemod.2012.10.007.
- 993 Peliz, A., Dubert, J., Marchesiello, P., Teles-Machado, A., 2007. Circulation
994 in the Gulf of Cadiz: Model and mean flow structure. *J. Geophys. Res.*
995 112, C11015. doi:10.1029/2007JC004159.

- 996 Peliz, A., Teles-Machado, A., Marchesiello, P., Dubert, J., Lafuente,
997 J.G., 2009. Filament generation off the Strait of Gibraltar in re-
998 sponse to Gap winds. *Dynamics of Atmospheres and Oceans* 46, 36–45.
999 doi:10.1016/j.dynatmoce.2008.08.002.
- 1000 Penven, P., Marchesiello, P., Debreu, L., Lefèvre, J., 2008. Software tools for
1001 pre- and post-processing of oceanic regional simulations. *Environmental*
1002 *Modelling Software* 3, 660–662. doi:10.1016/j.envsoft.2007.07.004.
- 1003 Pichevin, T., Nof, D., 1996. The eddy cannon. *Deep-Sea Res. I* 43, 1475–1509.
- 1004 Richardson, P.L., Bower, A., Zenk, W., 2000. A census of meddies tracked
1005 by floats. *Progress in Oceanography* 45, 209–250.
- 1006 Richardson, P.L., McCartney, M.S., Maillardi, C., 1991. A search for meddies
1007 in historical data. *Dynamics of Atmospheres and Oceans* 15, 241–265.
- 1008 Richardson, P.L., Tychensky, A., 1998. Meddy trajectories in the Canary
1009 Basin measured during the Semaphore Experiment, 1993-1995. *J. Geo-*
1010 *phys. Res.* 103, C11, 25029–25045.
- 1011 Richardson, P.L., Walsh, D., Armi, L., Schroder, M., Price, J., 1989. Tracking
1012 three meddies with SOFAR floats. *J. Physical Oceanogr.* 19, 371–383.
- 1013 Sanz, J.L., Acosta, J., Esteras, M., Herranz, P., Palomo, C., Sandoval, N.,
1014 1991. Prospección geofísica del Estrecho de Gibraltar (Resultados del pro-
1015 grama Hércules 1980-1983). *Publicaciones especiales del Instituto Español*
1016 *de Oceanografía. Instituto Español de Oceanografía.*
- 1017 Serra, N., Ambar, I., 2002. Eddy generation in the Mediterranean Undercur-
1018 rent. *Deep-Sea Res. II* 49, 4225–4243.
- 1019 Serra, N., Ambar, I., Käse, R., 2005. Observations and numerical mod-
1020 elling of the Mediterranean outflow splitting and eddy generation. *Deep-*
1021 *Sea Res. II* 52, 383–408.
- 1022 Serra, N., Sadoux, S., Ambar, I., Renouard, D., 2002. Ob-
1023 servations and laboratory modeling of meddy generation at Cape
1024 St. Vincent. *J. Physical Oceanogr.* 32, 3–25. doi:10.1175/1520-
1025 0485(2002)032;0003:OALMOMj2.0.CO;2.

- 1026 Shapiro, G.I., Meschanov, S.L., 1996. Spreading pattern and mesoscale struc-
1027 ture of Mediterranean outflow in the Iberian Basin estimated from histor-
1028 ical data. *J. Marine Sys.* 7, 337–348.
- 1029 Shchepetkin, A., McWilliams, J., 2003. A method for computing horizon-
1030 tal pressure-gradient force in an oceanic model with a nonaligned vertical
1031 coordinate. *J. Geophys. Res.* 108, C3, 35–1.
- 1032 Shchepetkin, A.F., McWilliams, J.C., 2005. The regional oceanic model-
1033 ing system (ROMS): a split-explicit, free-surface, topography-following-
1034 coordinate oceanic model. *Ocean Modelling* 9, 347–404.
- 1035 Smith, W., Sandwell, D., 1997. Global Sea Floor Topography from Satel-
1036 lite Altimetry and Ship Depth Soundings. *Science* 277, 1956–1962.
1037 doi:10.1126/science.277.5334.1956.
- 1038 Zenk, W., Schultz-Tokos, K., Boebel, O., 1992. New observations of meddy
1039 movement south of Tejo plateau. *Geophys. Res. Lett.* 19, 2389–2392.